ARTICLE

Tectonics and sedimentation of the central sector of the Santo Onofre rift, north Minas Gerais, Brazil

Tectônica e sedimentação do setor central do rifte Santo Onofre, norte de Minas Gerais, Brasil

Alice Fernanda Costa[1]*, André Danderfer Filho[2]

ABSTRACT: The Santo Onofre Group registers the filling of a Tonian, intracontinental paleo-rift that developed along the northern and central Espinhaço regions. This paper examines this unit in the central Espinhaço region with stratigraphic analysis and U-Pb geochronology, reviewing and dividing into the Canatiba and Rio Peixe Bravo Formations, which include the Barrinha Member. The Canatiba Formation mainly comprises carbon-rich mudstones that were deposited through low-density turbidity flows that alternated with sediment settling under anoxic conditions. The Rio Peixe Bravo Formation consists of a succession of sandstones and minor mudstones, which were deposited through low- to high-density turbidity flows. The Barrinha Member mainly consists of conglomerates and is related to channelized debris flows. Detrital zircon grains show maximum depositional ages of 930 ± 33 Ma and around 865 Ma for the Canatiba and Rio Peixe Bravo Formations, respectively. We interpret the Santo Onofre rifting to be relative younger than that for the Sítio Novo Group and to be a precursor stage of the glacial and post-glacial rift-to-passive margin-related sequences of the Macaúbas Group. The lithostratigraphic term "Macaúbas Supergroup" would be of better use to accommodate the unconformity-bounded Tonian sequences that were related to the Rodinia breakup in the Congo-São Francisco paleocontinent.

KEYWORDS: Rodinia supercontinent; Santo Onofre rift; Tonian; Macaúbas basin.

RESUMO: *O Grupo Santo Onofre registra o preenchimento de um paleorifte intracontinental Toniano desenvolvido ao longo do Espinhaço setentrional e central. Este trabalho analisa essa unidade no Espinhaço central a partir de trabalho de campo, análise estratigráfica e geocronologia U-Pb, revisando-o e dividindo-o nas formações Canatiba e Rio Peixe Bravo, que inclui o Membro Barrinha. A Formação Canatiba compreende principalmente pelitos carbonosos, maciços e laminados, depositados principalmente por fluxos turbidíticos de baixa densidade que alternaram com decantação de sedimento em suspensão em condições anóxidas. A Formação Rio Peixo Bravo consiste de uma sucessão de arenitos grossos a finos com subordinados pelitos, que foram depositados a partir de fluxos turbidíticos de alta a baixa densidade. O Membro Barrinha foi distinguido em dois corpos que consistem principalmente de conglomerados com arenitos subordinados, relacionados a fluxo de detritos canalizados. Grãos de zircões detríticos extraídos desta unidade mostram idade máxima de deposição de 930 ± 33 Ma e em torno de 865 Ma para as formações Canatiba e Rio Peixe Bravo, respectivamente. O rifte Santo Onofre é relativamente mais jovem do que o rifte que acolheu o Grupo Sítio Novo e um estágio precursor das sequências glacial e pós-glacial do Grupo Macaúbas. O termo litoestratigráfico "Supergrupo Macaúbas" utilizado é proposto para acomodar as sequências tonianas que ocorrem ao longo da serra do Espinhaço, no interior do paleocontinente São Francisco, e que estavam relacionadas à quebra do Supercontinente Rodínia.*

PALAVRAS-CHAVE: *Supercontinente Rodínia; rifte Santo Onofre; Toniano; Bacia Macaúbas.*

[1]Graduate Program of Department of Geology, Mine School, Universidade Federal de Ouro Preto – UFOP, Ouro Preto (MG), Brazil. *E-mail: alicecosta09@gmail.com*

[2]Department of Geology, Mine School, Universidade Federal de Ouro Preto – UFOP, Ouro Preto (MG), Brazil. *E-mail: danderferandre@gmail.com*

*Corresponding author.

INTRODUCTION

Important tectonic cycles occurred during the Proterozoic Eon, including orogenic events such as the Grenvillian Cycle (ca. 1,200 – 1,000 Ma, Gower & Krogh 2002, Li *et al.* 2008, Cordani *et al.* 2010). The Rodinia Supercontinent was formed during the Late Mesoproterozoic and Early Neoproterozoic Eras (Hoffman 1991, Meert 2001, Li *et al.* 2008). Several phases that involved the breaking of Rodinia occurred, either through passive or active rifting, which were induced by remotely applied tensions (in-plane stress) and mantle plumes, respectively (Li *et al.* 2008, Ernst *et al.* 2008). These processes operated diachronically through a continental mass, and the full disintegration of the continent was complete at the end of the Tonian Period (Hoffman 1991, Li *et al.* 2008, Cawood *et al.* 2016). Many rifts were formed before reaching this stage, some of which were aborted, and mafic dyke swarms intruded, which became dispersed in the scattered continents (Chew *et al.* 2010, Volkert *et al.* 2015). Investigations of these features have provided a better understanding of the space-temporal evolution of the Rodinia, for reconstructions (Hoffman 1991, Meert 2001, Li *et al.* 2008).

The Congo-São Francisco paleocontinent is characterized as one of several fragments of the Rodinia (Hoffman 1991, Li *et al.* 2008). This paleocontinent encompasses the cover and basement rocks of São Francisco and Congo cratons and their marginal orogenic belts (Fig. 1; Almeida 1977, Alkmim *et al.* 1993, Trompette 1994). The Espinhaço mountain range is a remarkable feature that extends with a sub-meridian direction across the entire extent of the Congo-São Francisco paleocontinent. The southern and central Espinhaço range regions integrate the Araçuaí fold and thrust belt as one of the external domains of the Neoproterozoic Araçuaí-West Congo orogen (Almeida 1977, Pedrosa-Soares *et al.* 1992, 1998, 2001, 2008, Alkmim *et al.* 2006, 2017), while the northern extension occurs along the eastern border of the Paramirim aulacogen, which was partially inverted, and involves the basement in the cover deformation (Schobbenhaus 1993, 1996, Danderfer 2000, Alkmim *et al.* 1993, Cruz & Alkmim 2006, 2017, Fig. 1).

Several unconformity-bounded stratigraphic successions have been characterized along southern and central Espinhaço regions and within the Paramirim aulacogen (Schobbenhaus 1996, Pedrosa-Soares *et al.* 2001, Danderfer & Dardenne 2002, Chemale Jr. *et al.* 2012, Danderfer *et al.* 2009, 2015, Alkmim & Martins-Neto 2012, Guadagnin *et al.* 2015, Cruz & Alkmim 2017). Each unconformity-bounded unit has been considered a record of an episode of basin formations within the Congo-São Francisco paleocontinent, beginning at 1.8 Ga. Generally, the Paleo-Mesoproterozoic-age units are mapped as Espinhaço Supergroup, and those of Neoproterozoic age are attributed to the supergroup of São Francisco (Schobbenhaus 1996, Martins-Neto *et al.* 2001, Danderfer & Dardenne 2002, Alkmim & Martins-Neto 2012).

The sequences mapped to be adjacent to and along the northern and central Espinhaço regions trend N-S and end abruptly against the Macaúbas Basin, along the southern edge of the central Espinhaço range (Fig. 1). This basin corresponds to a rift that evolved to a passive margin within the Congo-São Francisco paleocontinent as a paleo-gulf, and was under glaciogenic influence during filling (Noce *et al.* 1997, Uhlein *et al.* 2007, Pedrosa-Soares *et al.* 1992, 1998, 2001, 2011, Babinski *et al.* 2012, Kuchenbecker *et al.* 2015). According to Schobbenhaus (1996) and Danderfer and Dardenne (2002), the last basin-formation event along the northern Espinhaço range is represented by the siliciclastic, unconformity-bounded unit of Santo Onofre Group. These authors suggested a space-time correlation of this unit with those that built up the filling of Macaúbas Basin, but there are no studies on the central Espinhaço region to better establish this relationship.

We must examine the units along the central Espinhaço range to better understand the evolution and age of the sedimentary filling of the Santo Onofre paleo-basin. This study presents stratigraphic analyses and U-Pb geochronological data on detrital zircons in the southern-central segment of Santo Onofre Group along a portion of the central Espinhaço (north of Minas Gerais, eastern Brazil). The data enable us to characterize the stratigraphic architecture, depositional processes, and maximum ages of Santo Onofre Group. The results allow us to discuss the different outcropping domains of this unit along northern and central Espinhaço and the Macaúbas Group, and present a new stratigraphic proposal for the investigated area.

REGIONAL STRATIGRAPHY

Few sources of information exclusively deal with the detailed study of the stratigraphy of the northern portion of the central Espinhaço range. Some proposals were presented for the upper sedimentary succession in this region based on the stratigraphy of Santo Onofre Group, with others based on the stratigraphy of Macaúbas Group. Both units were originally defined and best investigated along the northern Espinhaço and to the south of the central Espinhaço range, respectively. We present an update to the lithostratigraphic framework of each region to discuss the stratigraphic problems in the investigated area (Fig. 2).

Northern Espinhaço

The term "Santo Onofre Group" was introduced by Schobbenhaus (1972) to refer to all the volcanic and sedimentary rocks from the northern Espinhaço. Based on a compilation of several geological mapping projects, Schobbenhaus (1993) redefined the stratigraphy of this region and restricted the use of the term "Santo Onofre Group" to the upper interval of the sedimentary succession, which comprises the Santo Onofre and Sítio Novo Formations of Inda and Barbosa (1978). Schobbenhaus (1996) correlated the redefined Santo Onofre Group to Macaúbas Group, and interpreted this unit as the filling of a failed Tonian rift.

Danderfer (2000) performed a detailed tectonostratigraphic analysis and recognized and characterized eight
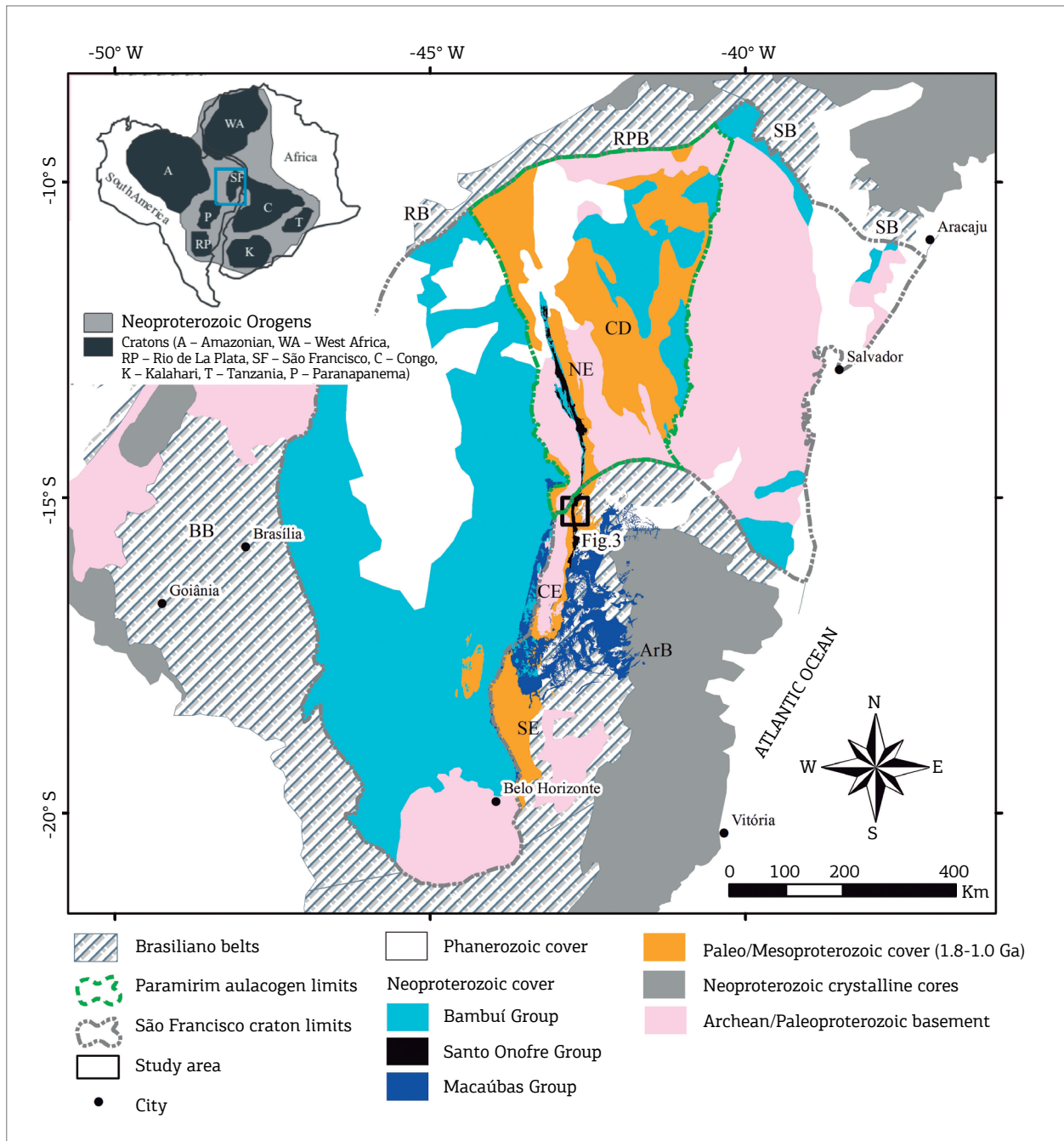
Figure 1. Simplified geologic map of the São Francisco craton and adjacent Brasiliano belts: Rio Preto (RB), Riacho do Pontal (RPB), Sergipano (SB), Araçuaí (ArB), and Brasília (BB). The inset indicates the location of the map in the tectonic scenario of West Gondwana (modified from Danderfer *et al.*, 2015). Chapada Diamantina (CD), Northern Espinhaço (NE), Central Espinhaço (CE) and Southern Espinhaço (SE).

unconformity-bounded units along the northern Espinhaço. The results enabled Danderfer and Dardenne (2002) to redefine the lithostratigraphic framework of this region based on the stratigraphic code (Fig. 2). According to the new proposal, the two youngest unconformity-bounded units correspond to the Sítio Novo and Santo Onofre groups, which were separated through an erosive and angular unconformity; both groups were included in the Santo Onofre Group from Schobbenhaus (1996).

According to Danderfer and Dardenne (2002), the Sítio Novo Group records a precursor rift stage that was generated by single-extensional tectonics, while the Santo Onofre Group records the last rifting event, which was related to strike-slip tectonics. The NNE-SSW Santo Onofre fault, which has moderate to high dip to the east, nucleated as a master fault during the Sítio Novo rift's formation and then reactivated during the Santo Onofre rifting (Danderfer 2000). Detrital zircons were dated and given a maximal deposition age from 938 to 828 Ma for Sítio Novo and Santo Onofre Groups, respectively (Sousa *et al.* 2014). Several mafic dikes and sills were found in the northern Espinhaço, but none

intruded the Sítio Novo and Santo Onofre successions. Danderfer *et al.* (2009) reported one mafic dyke with an age of 854 ± 23 Ma (U-Pb SHRIMP), and suggested that this dike was related to the Santo Onofre rifting.

Danderfer and Dardenne (2002) subdivided Santo Onofre Group into three formations, which were laterally and vertically complexly interdigitated and had distinct lithofacies successions (from the base to the top): the Canatiba Formation (carbonaceous, laminated and massive mudstones), Boqueirão Formation (sandstones with minor carbonaceous, laminated and massive mudstones), and João Dias Formation (mainly conglomerates and breccias with minor sandstones and mudstones). According to Danderfer and Dardenne (2002), the deposition of Santo Onofre Group would have been associated with gravity flows in a deep-water environment without direct glacial influence.

Dominguez and Rocha (1989) mapped four depositional systems between the central and northern Espinhaço ranges (from the base to the top): Baixão, Salto, Telheiro and Gentio. According to Danderfer (2000), the Telheiro and Salto depositional sequences correspond to Sítio Novo Group, and the
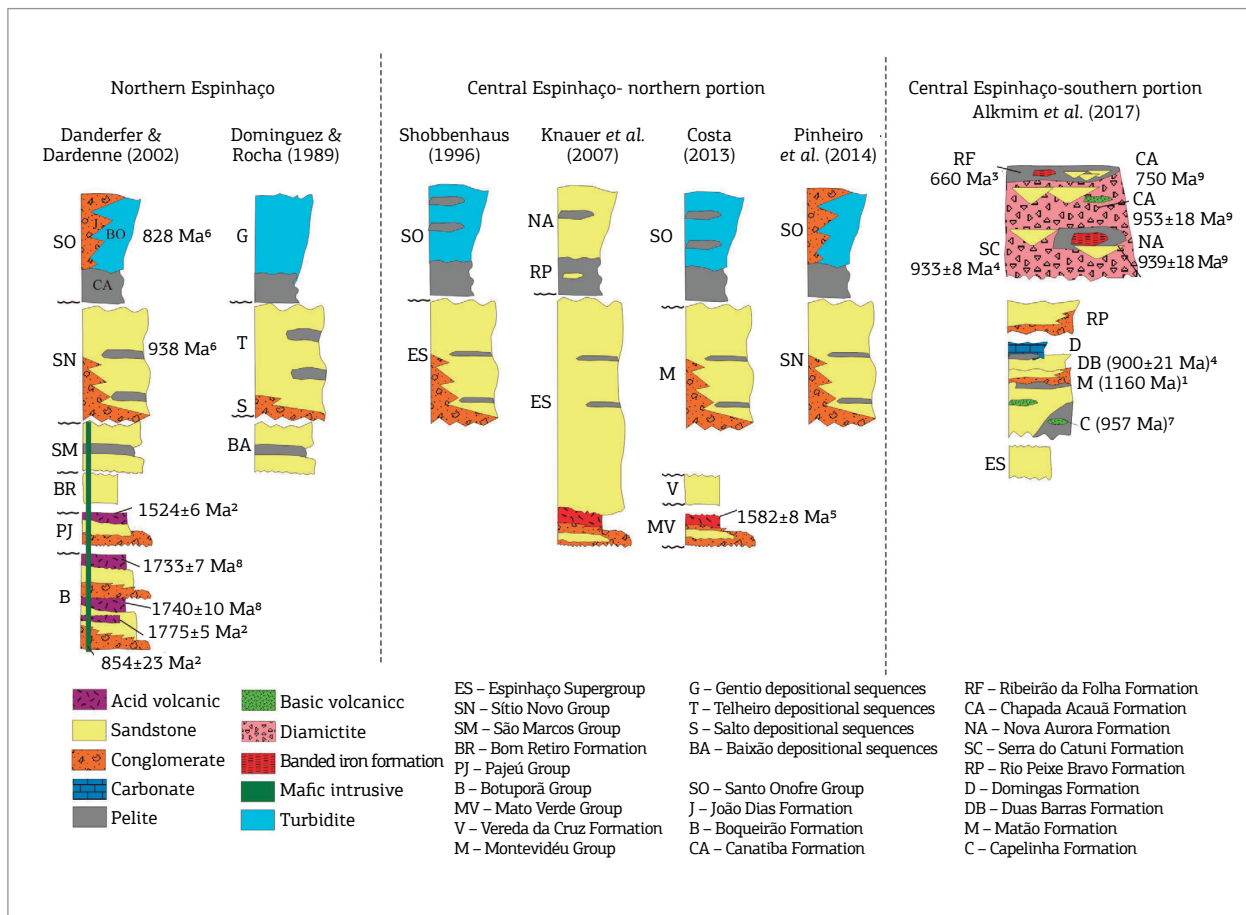
Figure 2. Stratigraphic columns produced by previous studies in different regions. Ages: [1]Martins *et al.* (2008), [2]Danderfer *et al.* (2009), [3]Queiroga (2010), [4]Babinski *et al.* (2012), [5]Costa *et al.* (2014), [6]Sousa *et al.* (2014), [7]Castro (2014), [8]Danderfer *et al.* (2015), [9]Kuchenbecker *et al.* (2015).

Gentio depositional sequence to Santo Onofre Group, based on similar sedimentary characteristics and stratigraphic positions.

Central Espinhaço – southern portion

Macaúbas Group represents a Neoproterozoic metasedimentary succession, which is separated from Espinhaço Supergroup by an erosional unconformity (Martins *et al.* 2008). The name "Macaúbas" has been previously used by Moraes (1929) and Moraes and Guimarães (1931) to describe only the diamictite-bearing units. The concept of "groups" has been expanded to integrate non-glacial units (Karfunkel *et al.* 1985, Pedrosa-Soares *et al.* 1992, Noce *et al.* 1997, Martins *et al.* 2008). Recent geochronological dating has provided a new view of Macaúbas' stratigraphy and basin evolution (Babinski *et al.* 2012, Castro 2014, Kuchenbecker *et al.* 2015, Sousa 2016).

Classically, Macaúbas Group has been subdivided into three major sequences (Fig. 2): pre-glacial, glaciogenic and post-glacial sequences (Pedrosa-Soares *et al.* 2011, Babinski *et al.* 2012, Kuchenbecker *et al.* 2015). The pre-glacial sequence includes Capelinha, Matão, Duas Barras, Domingas and Rio Peixe Bravo Formations, which were deposited in continental to shallow-marine environments during rifting (Martins *et al.* 2008, Pedrosa-Soares *et al.* 2011, Castro 2014, Kuchenbecker *et al.* 2015, Cruz & Alkmim 2017). Some distinct episodes of anorogenic magmatism are associated with this rifting succession:

- tholeiitic metabasalts interbedded in Capelinha Formation (957 Ma, Castro 2014);
- Pedro Lessa mafic dykes (c. 933 Ma, Queiroga *et al.* 2012; 939 ± 7, Sousa 2016);
- the A-type granites of Salto da Divisa Suite (c. 875 Ma, Silva *et al.* 2008; Menezes *et al.* 2012); and
- Pedra Preta Amphibolite (Gradim *et al.* 2005).

The U-Pb detrital zircon ages are compatible with a rift-related magmatism and indicate a maximum depositional age of 970 Ma (Castro 2014), 1,160 Ma (Martins *et al.* 2008), and 900 ± 21 Ma (Babinski *et al.* 2012) for Capelinha, Matão and Duas Barras Formations, respectively. The age spectrum of detrital zircons from Rio Peixe Bravo record a contribution from Rhyacian sources, which were possibly related to Porteirinha Complex (Babinski *et al.* 2012); the youngest age obtained was 1,578 Ma.

The glaciogenic sequence is separated from the pre-glacial sequence by a regional unconformity (Karfunkel & Hoppe 1988; Uhlein *et al.* 1998, 1999, Martins-Neto *et al.* 2001), which separates two different basin-forming events (Kuchenbecker *et al.* 2015). The glaciogenic sequence comprises diamictite-rich packages of Serra do Catuni, Nova Aurora and Lower Chapada Acauá Formations (Noce *et al.*

1997, Pedrosa-Soares *et al.* 2011). Locally, a Rapitan-type diamictitic iron formation has occurred in Nova Aurora Formation (Viveiros *et al.* 1978, Uhlein *et al.* 1999, Vilela *et al.* 2014). U-Pb detrital zircon ages indicate a maximum depositional age of 933 ± 8 Ma, 939 ± 18 Ma, and 953 ± 18 Ma from Serra do Catuni, Nova Aurora and Lower Chapada Acauá Formations, respectively (Babinski *et al.* 2012, Kuchenbecker *et al.* 2015).

The post-glacial sequence comprises the diamictite-free units in Upper Chapada Acauá and Ribeirão da Folha Formations (Pedrosa-Soares *et al.* 1992, 1998, 2011). The Upper Chapada Acauá comprises sandstone and mudstone, which were deposited in a shelf environment during the passive margin stage (Noce *et al.* 1997, Pedrosa-Soares *et al.* 2011). Detrital zircon grains from a quartzite suggest a maximum depositional age of around 750 Ma (Kuchenbecker *et al.* 2015). The Upper Chapada Acauá Formation passes laterally into Ribeirão da Folha Formation, which contains distal passive-margin and ocean-floor deposits (Pedrosa-Soares *et al.* 1992, 1998, 2011, Queiroga *et al.* 2007). Detrital zircon grains suggest a maximum depositional age of around 806 Ma (Peixoto *et al.* 2015). Metamafic and meta-ultramafic rocks with an ocean-floor lithochemical signature yielded Ediacaran magmatic crystallization U-Pb ages, which suggest oceanic spreading from at least ca. 660 to 600 Ma (Queiroga *et al.* 2007, Queiroga 2010).

Central Espinhaço – northern portion

Most of the current geological knowledge regarding central Espinhaço originated from regional mapping and integration works, which had conflicting stratigraphic classifications (Schobbenhaus 1972, 1993, Moutinho da Costa 1976, Bruni *et al.* 1976, Drumond *et al.* 1980, Fernandes *et al.* 1982, Souza *et al.* 2003, Knauer *et al.* 2007). This region is sectioned by the southern extension of Santo Onofre Fault, which divides the area into two blocks (eastern and western) with distinct stratigraphic characteristics.

Previously, the volcano-sedimentary succession on the western block was attributed to Espinhaço Supergroup (Schobbenhaus 1996, Knauer *et al.* 2007). The stratigraphy of the western block was recently redefined by Costa (2013), based on the recognition and characterization of unconformities. The basal succession is represented by Mato Verde Group, which includes volcano-sedimentary rocks related to Calymmian rifting (1,524 ± 6 Ma, Costa *et al.* 2014). According to Costa (2013), Vereda da Cruz Formation corresponds to eolian sandstones, which are related to the infilling of an intracontinental sag basin. Lastly, the top of the overall sequence contains Montevidéu Formation, which is a rift basin-fill succession.

To the east of Santo Onofre Fault, Schobbenhaus (1996) distinguished quartzites and carbonaceous mudstones from

Espinhaço Supergroup and Santo Onofre Group, respectively. Knauer *et al.* (2007) recognized Macaúbas Group and considered the mapped area of Espinhaço Supergroup as Nova Aurora Formation, and Santo Onofre Group as Rio Peixe Bravo Formation. Recent geological mapping by Pinheiro *et al.* (2014) considered the proposal of Schobbenhaus (1993), but defined Sítio Novo Group in the area previously mapped as Espinhaço Supergroup.

MATERIALS AND METHODS

This work was based on 1:50.000 geological mapping, including a stratigraphic data survey to a base study of the facies and their associations (Fig. 3). We found well-preserved primary structures in several outcrops, mainly along the eastern portion, where less strained rocks occur. Metasedimentary rocks were described by using sedimentary-rock nomenclature for practical purposes and Miall's (1996) facies code for facies description and analysis. Microscopic information was added to the facies' descriptions.

A schematic, composite stratigraphic column was constructed from a combination of several individual large-scale, composite stratigraphic profiles and based on the distribution and structural orientation of the defined lithostratigraphic units along the geological map (Fig. 4). These profiles were located in the northern portion of the area, perpendicular to the strike of layers that form Santo Antônio Syncline, which is an upright, closed fold that gently plunges south (Fig. 3). The stratigraphic thickness for all the studied profiles was
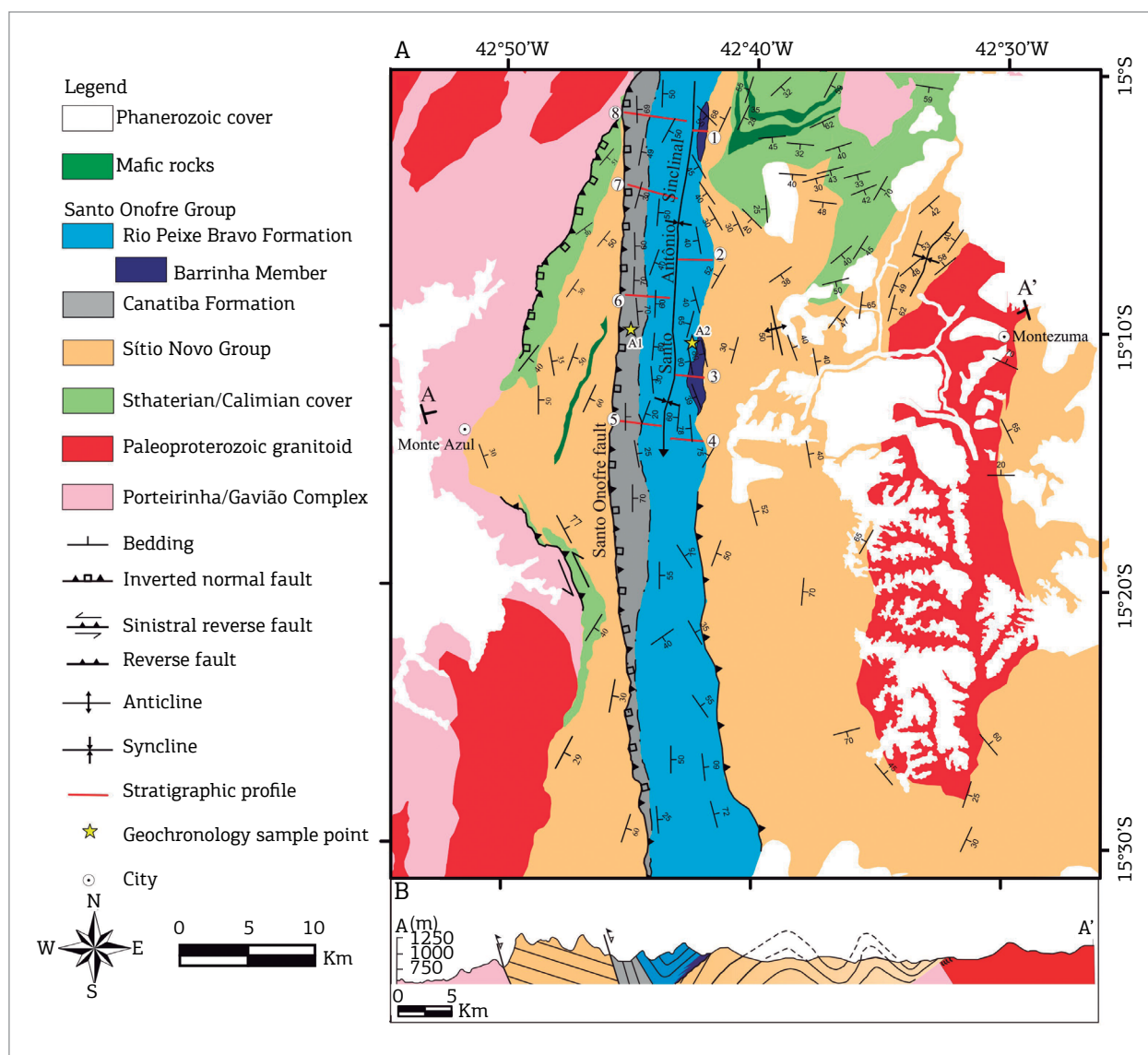
Figure 3. (A) Geological map of the study area with locations of the measured sections 1-8 and the samples analyzed for U-Pb geochronology; (B) Geological cross section across the study area (A-A') in a SW-NE direction.

estimated from indirect measurements following the methods in Ragan (2009). Then, the lithofaciological observations in scattered exposures around each profile were compiled and projected to the section line of each stratigraphic profile. The results and stratigraphic data enabled us to analyze and interpret the depositional process and the vertical and lateral relationships among the lithostratigraphic units, improving our understanding of the paleo-basin's architecture and infilling. The subdivision of the stratigraphic record in the study area and the regional stratigraphic correlations were based on the stratigraphic code (Petri *et al.* 1986, Salvador 1994).

Two samples were collected for geochronological analyses (Fig. 3A). Zircons were separated from rock samples for U-Pb analyses at the Department of Geology (DEGEO), Universidade Federal de Ouro Preto, Brazil. The zircon

extraction technique used a jaw crusher, milling, manual panning, hand-picking under a binocular microscope and mounting on 25 mm epoxy mounts. These mounts were polished and imaged under Scanning Electron Microscope (SEM) cathodoluminescence (CL) in a JEOL 6510 Scanning Electron Microscope, at the DEGEO.

The isotopic analyses were conducted by using a Thermo-Finnigan Element 2 sector field ICP-MS, coupled to a CETAC 213 ultraviolet laser system (LA-SF-ICP-MS) at the DEGEO. Data were acquired in peak-jumping mode during a 20 s background measurement, followed by a 20 s sample ablation with a spot size of 20 μm. These data were corrected for the background signal, common Pb, laser-induced elemental fractionation, instrumental mass discrimination and time-dependent elemental fractionation of Pb/U
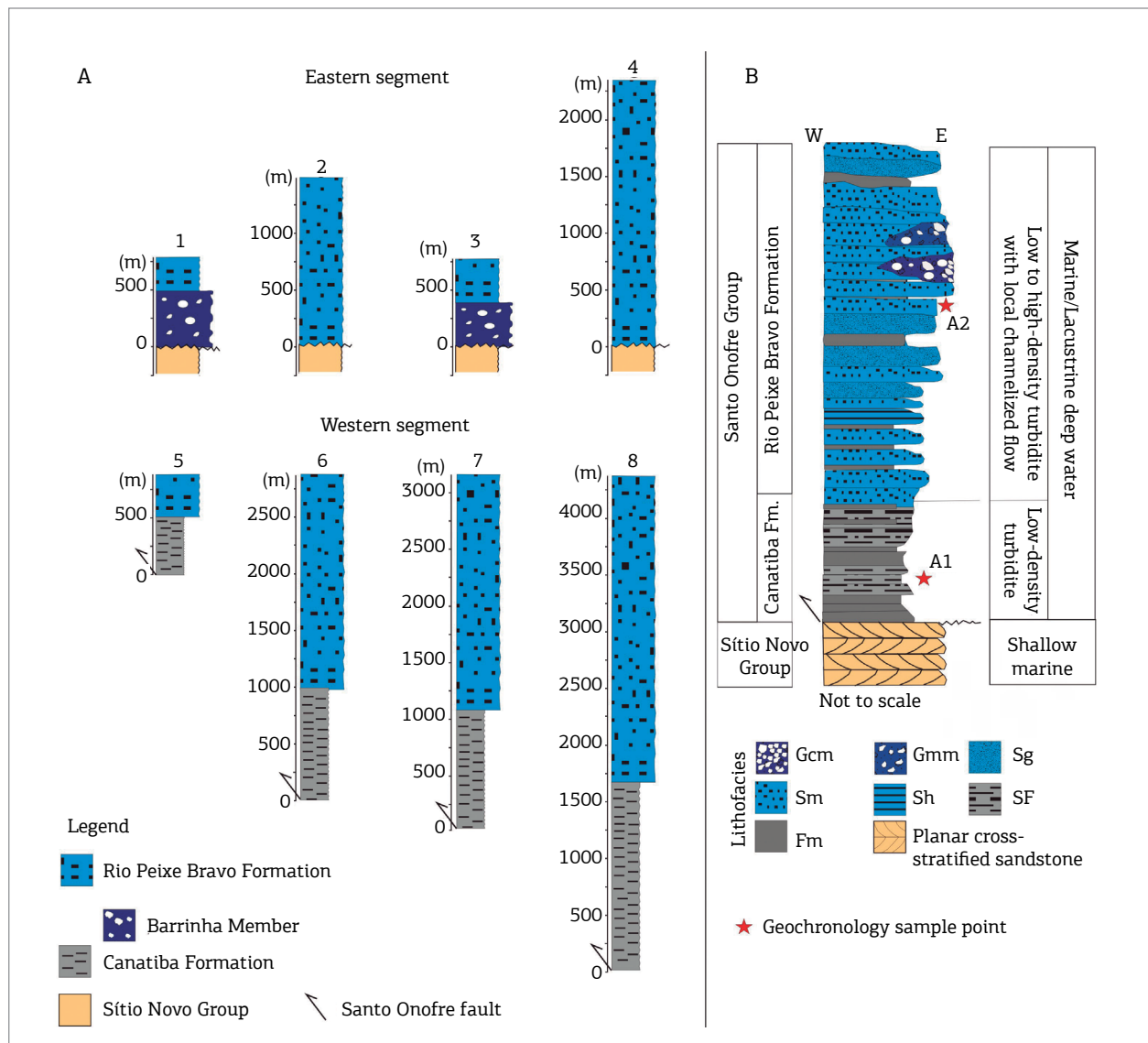
Figure 4. (A) General stratigraphic columns showing thickness for stratigraphic units (location shown in Fig. 3); (B) Generalized stratigraphic column of the Santo Onofre Group (facies distribution schematic).

by using an MS Excel spreadsheet program (Gerdes & Zeh 2006). We used the GJ-1 zircon (608 ± 1 Ma, Jackson *et al.* 2004) as the primary reference material and the Plešovice zircon (337 ± 1 Ma, Sláma *et al.* 2008) as a secondary standard for quality control. The signal data were reduced by using the Glitter software (van Achterbergh *et al.* 2001), and age-distribution diagrams were constructed by using Excel Isoplot program (Ludwig 2003).

Zircon ages which were >10% discordant were rejected in this study (Gehrels 2011). $^{206}U/^{238}Pb$ ages were used for analyses younger than 1,000 Ma, while $^{207}Pb/^{206}Pb$ ages were used for analyses older than 1,000 Ma. A complete discussion of the discordance cutoffs for provenance studies and strategies defining the maximum depositional age can be found in Spencer *et al.* (2016). The errors in the tables and figures were at the 1-sigma level.

STRATIGRAPHY

Stratigraphic framework

Our work emphasized the upper siliciclastic sequence occurred immediately to the east of Santo Onofre Fault (Fig. 3). The main stratigraphic problem previous authors have experienced in this region was the difficulty in differentiating between Santo Onofre and Macaúbas Groups and between their related lithostratigraphic formations. In the original setting areas, both units were deposited over an unconformity with Espinhaço Supergroup's rocks and show siliciclastic sedimentation with sand-mud rhythmites, mudstones (locally rich in graphite or carbonaceous material) and subordinate conglomerates (Schobbenhaus 1996, Noce *et al.* 1997, Danderfer & Dardenne 2002, Martins *et al.* 2008). Thus, we review the lithostratigraphic framework based on the sedimentary characteristics of the mapped units in the studied area. The stratigraphic definitions and subdivisions consider the lithofacies sedimentary characteristics and stratigraphic position that each succession exhibits alongside the boundary relationships among them. The sedimentary processes during their depositions and environment interpretation are then presented for each unit. We attempt to preserve traditional and well-established names. The rules of priority in denominations were satisfied, though some terms were redefined, while other new names were created.

The field data allowed us to distinguish two major lithostratigraphic units, represented by Espinhaço Supergroup and Santo Onofre Group (Fig. 3), as initially postulated by Schobbenhaus (1996). The contact between these units is marked by an angular unconformity, whose relationships could be observed in the northern portion of the area according to the difference between the bedding attitudes of

Espinhaço Supergroup (263/80) and Santo Onofre Group (256/35). To the south, an east-verging, reverse shear zone placed the rocks from Santo Onofre Group onto the rocks from Espinhaço Supergroup near the contact, obliterating the original relationships between both units (Fig. 3). We focus on the Santo Onofre succession, although some considerations are briefly made below regarding the underlying unit, which is still under investigation.

Espinhaço Supergroup comprises stratified sandstones and minor mudstones and conglomerates, with characteristics that indicate deposition in coastal to shallow-marine environments. Just below Santo Onofre Group, the top of Espinhaço Supergroup is marked by a thick succession predominantly consisting of low- to intermediate-angle planar-cross-stratified, medium- to thick-bedded, medium to fine sandstones with minor thin mudstone, which is interpreted as a shallow-marine facies succession. In addition, the overall siliciclastic succession of Espinhaço Supergroup in the studied area presents physical continuity to the north, with the Salto and Telheiro depositional sequences, recognized by Dominguez and Rocha (1989) as continental and shallow-marine deposits, respectively. Both sequences were correlated and mapped as components of Sítio Novo Group, in the northern Espinhaço region, by Danderfer (2000), with the same depositional characteristics (Fig. 2). The extent of Espinhaço Supergroup corresponds almost integrally to the area mapped by Knauer *et al.* (2007) as Nova Aurora Formation, although there is no evidence of sedimentation influenced by glaciation, such as glaciogenic diamictites, at the typical localities of this unit (Uhlein *et al.* 1999, Pedrosa-Soares *et al.* 2011, Babinski *et al.* 2012). There is no justification for such a correlation; therefore, we retain the term Espinhaço Supergroup and endorse a correlation with Sítio Novo Group.

The mapped Santo Onofre Group constitutes the portion of Rio Peixe Bravo Formation, defined by Knauer *et al.* (2007), or a large portion of Santo Onofre Formation by Souza *et al.* (2003). In addition, this group was considered as Canatiba Formation by Fernandes *et al.* (1982) and Espinhaço Supergroup by Bruni *et al.* (1976). The western contact is limited by the Santo Onofre fault (Fig. 3). We divided Santo Onofre Group into two formations based on the predominant facies associations: Canatiba and Rio Peixe Bravo (Figs. 3 and 4). The facies variations of each unit suggest transitional boundaries between them, with contacts arbitrarily located within intergrading zones or the complex intertonguing of facies.

The regional profiles on both sides of the Santo Antônio syncline (Fig. 3B) — which is located to the north of the area, where rocks are less deformed —, allowed us to infer the relative stratigraphic positioning and relationships of

each formation of Santo Onofre Group. The Canatiba succession (predominantly mudstone with subordinate sandstone intercalations) occurs along the western portion of the mapped area, close to the Santo Onofre fault, according to an N-S strip with an average width of 2 km on the map and an apparent thickness of 583 m; the real thickness could not be evaluated due to the greater deformation of this succession close to the fault (Figs. 3 and 4). Canatiba Formation presents physical continuity and is similar to the homonymous unit-stratotype, redefined by Danderfer (2000) in the northern Espinhaço; therefore, this name was retained. The facies association of Canatiba Formation passes vertically and laterally to the east to Rio Peixe Bravo Formation.

Rio Peixe Bravo Formation (mainly sandstone and minor mudstone beds, with disperse conglomerate lenses) occurs along the eastern area over Espinhaço Supergroup according to an N-S strip, with an average width of 4.5 km on the map and a minimal thickness of 276 m (Figs. 3 and 4). Regional shortening caused Santo Onofre Group to be closely folded, and the subsequent erosive effect destroyed the sedimentary record of Rio Peixe Bravo Formation at the top and laterally on both sides of the Santo Antônio syncline (Fig. 3B). Thus, we could not evaluate the facies behavior of this unit towards Santo Onofre fault or its extension to the east. Rio Peixe Bravo Formation was originally defined as a basal unit of Macaúbas Group by Viveiros *et al.* (1978). This unit was not found within the type area of Macaúbas Group (Noce *et al.* 1997, Pedrosa-Soares *et al.* 1998, 2011, Babinski *et al.* 2012), but occurs along the area that comprises Santo Onofre Group; this formation was included in the latter. The facies associations of Rio Peixe Bravo resemble those described by Danderfer and Dardenne (2002), in Boqueirão Formation, northern Espinhaço, although without physical continuity.

In this work, we introduce Barrinha Member as a distinct rock unit within Rio Peixe Bravo Formation, which was not detected in previous works and mainly includes conglomerate and minor sandstone and mudstone beds. This member was mapped as two discontinuous and lenticular bodies with an N-S orientation directly over Espinhaço Supergroup and laterally interdigitated with the facies associations of Rio Peixe Bravo Formation (Fig. 3). Both bodies show an average width of 1 km on the map and a maximal thickness of 450 m (Fig. 4). The most typical section lies near the Barrinha stream (Fig. 3). A similar conglomerate deposit to the Barrinha Member was described by Danderfer and Dardenne (2002) in João Dias Formation, northern Espinhaço, and was related to Santo Onofre rift faulting. A fundamental difference between these units is their spatial positioning. Barrinha Member occurs along the eastern border of Santo Onofre Group, while João Dias Formation

occurs along the western border as a fringe deposit associated with the Muquém fault.

Facies and facies associations

The textural and compositional characteristics, the sedimentary structures and the geometry of the layers enabled us to identify seven lithofacies within Santo Onofre Group (Tab. 1). These facies were grouped into facies associations to define the three successions of dominant facies in the studied area related to each stratigraphic unit in Santo Onofre Group.

Facies association of Canatiba Formation (FA1)

FA1 mainly consists of very fine-grained facies, which are predominant in mudstone and comprise less than 20% of sandstone. This formation essentially consists of massive carbon-rich mudstones (lithofacies Fm, Fig. 5A) and interbedded millimeter- to centimeter-thick alternations of very fine sandstone and mudstone (lithofacies SF, Fig. 5B). The geometry of each bed is tabular or sheet-like, and each bed is found in packages up to 100 m thick. The contacts between Fm and SF lithofacies are usually sharp and non-erosive. The massive mudstone mainly occurs in the base of the succession. The profile of this succession shows a volumetric growth of the sand fraction towards the top, which suggests a coarsening-upward facies succession (Fig. 5C).

FA1 is interpreted to have been deposited from low-density turbidity flows that alternated with clay falling out of suspension in deep water from a lake or ocean (Lowe 1982, Mutti 1992). The high proportion of fine-grained sediment particles in very thin to medium bedding with sheet-like tabular geometry supports this interpretation. The presence of laminated mudstones is interpreted to record the deposition of the diluted portion of a waning sediment gravity flow across the shelf-to-slope transition (Mulder *et al.* 2003, Zavala & Arcuri 2016). The carbon-rich mudstones are more common in the lower area of the succession, suggesting deposition in a more distal or deep-water setting under quieter conditions (Talling *et al.* 2012, Zavala & Arcuri 2016).

Generally, the rocks from FA1 are highly strained near the Santo Onofre fault, with east-dipping, high-angle phyllitic cleavage, which is commonly associated with tight to isoclinal foldings; the layering appears parallel with the foliation. In this context, strain bands and crenulation cleavage related to the progressive deformation of the sediment pile are common. Away from this fault are less-deformed rocks with cleavage exhibiting low to moderate angles with the bedding. FA1's rocks were affected by low metamorphism, with levels yielding sericite and porphyroblasts of magnetite. Sandstones present cleavage domains defined by quartz-sericite composition with subordinate plagioclase in

thin sections (Fig. 5D). The pelitic portions mostly consist of sericite with opaque minerals and chloritoid in idioblastic grains, which are tabular to fine needle-shaped and overgrow the foliation (Fig. 5E).

Facies association of Rio Peixe Bravo Formation (FA2)

This association predominantly consists of sandstones, mainly Sm lithofacies and sometimes with graded or parallel-laminated, pebbly sandstone beds (Sg and Sh lithofacies). Conglomerate and mudstone lenses locally occur (Gmm and Fm lithofacies).

Individual Sm lithofacies sets show a minimum thickness of 0.5 – 2 m and tabular or amalgamated geometry (Fig. 6A). Thicker beds are usually separated by very thin layers of mudstones. Minor interbedded conglomerate lenses sometimes occur where basal contact is erosional (Fig. 5B). Generally, the polymict conglomerate beds (Gmm lithofacies) contain pebble- to cobble-grade, angular to sub-rounded clasts in a disorganized framework. The clast composition mainly consists of sandstone, quartz veins and mudstone. The mudstone clasts are located along discrete horizons, typically towards the bed's base (Fig. 6C). Sg and Sh lithofacies occur locally and are sometimes interbedded with mudstone lenses (Fig. 6D). The FA2 association

exhibits an overall thickening- and/or coarsening-upward trend (Figs. 6C and 6D).

In thin sections, the matrix of conglomerates is a poorly sorted coarse to very coarse sandstone, sometimes being granule sandstone containing quartz, lithic clasts of quartz, sandstone and mudstone (Fig. 6E). Generally, the sandstone's composition ranges from quartz arenite to sublitharenite. Opaque minerals occur as fine grains and occupy the interstitial space between the major grains of quartz.

FA2 is interpreted as having been transported by turbidity flows, that transformed from originally hyper-concentrated flows (Mulder & Alexander 2001, Haughton *et al.* 2009). The progressive changes in flow involved high initial charge, formed during high- to low-density flow. The coarse- to medium-grained lithofacies (Sm, Sg, Sh and Gmm) represent the deposits of high-density turbidity flows, and the thin-bedded mudstones represent the deposits of lower-density turbidity flows. The Sm and Sg lithofacies are interpreted as high concentrations of grains, which rapidly flowed on a slope and were quickly deposited under an upper-flow regime (Lowe 1982, Mutti 1992). The Sh lithofacies suggest a decrease in flow velocity, resulting in rapid deposition from high rates of suspension

Table 1. Summary of facies description and interpretation.

Code	Lithofacies	Description	Processes
Gcm	Massive clast-supported conglomerate	Disorganized, very poorly-sorted, dominantly clast supported to locally matrix suppported, polymictic conglomerate. Clasts ranging pebbles to boulders of sandstone and vein quartz, sub-rounded to angular; poorly sorted sandy matrix.	Non-cohesive hyperconcentrate debris flow (Lowe, 1982; Mulder & Alexander, 2001)
Gmm	Massive matrix-supported conglomerate	Polymictic conglomerate, ranging from granules to boulders of sandstone, mudstone and vein quartz, sub-rounded to angular, scattered in sandy-muddy matrix.	Cohesive debris flow (Lowe, 1982; Mutti, 1992)
Sg	Normal graded sandstone	Fine to coarse-grained sandstone, poorly sorted, composed of quartz, feldspar and muscovite. Normal graded, tabular geometry with erosional base, flat top with thicknesses of up to 1m	High-density turbidity flows (Lowe, 1982; Mutti, 1992)
Sh	Horizontally stratified sandstone	Fine- to medium-grained sandstone, moderately sorted, lenticular geometry from 0,3 to 1 m. Planar-horizontal to undulate lamination, sometimes normal graded.	Low-density turbidity flows or with reworked traction carpet (Lowe, 1982; Mutti, 1992)
Sm	Massive sandstone	Fine- to coarse-grained sandstone, moderately sorted, massive, tabular geometry with thickeness from 0,2 to 0,5 m and extensive lateral continuity.	Rapid deceleration of high density turbidity flows (Mutti, 1992; Talling *et al.*, 2012)
Fm	Massive mudstone	Massive mudstone, carbonaceous or not, bed with extensive lateral continuity (>50m), forming tabular strata from 0,5 to 5m in thickness.	Precipitation from suspension turbidite flows (Mutti, 1992; Talling *et al.*, 2012)
SF	Sandstone and mudstone thin laminated	Rhythimic alternation of mudstone/siltstone and fine sandstone, forming tabular beds up 10 cm thick, with a parallel lamination.	Low-density turbidity flows (Lowe, 1982)

fall-out from sustained flows (Mulder & Alexander 2001). The presence of conglomerates with mudstone clasts and the erosional base in some outcrops indicate highly turbulent erosive flows. Medium- to coarse-grained sandstone turbidites that comprise some thick-bedded, amalgamated and tabular geometry suggest a lobe deposit (Mutti 1992, Haughton *et al.* 2003, 2009). The thickening-upward cycles may indicate an increase in the strength/volume of turbidity currents over time, and suggest that these sequences were deposited in sloped and slope-rise submarine fans (Prélat *et al.* 2009).

FA2's rocks are poorly strained, with pressure solution-dominated cleavage transversal to well-preserved bedding. Interlayered mudstones exhibit more prominent deformations. However, along the southern contact with Espinhaço Supergroup, FA2's rocks are highly transposed and refolded by a second phase of progressive deformation from thrusting to the east; the original bedding planes cannot be recognized.
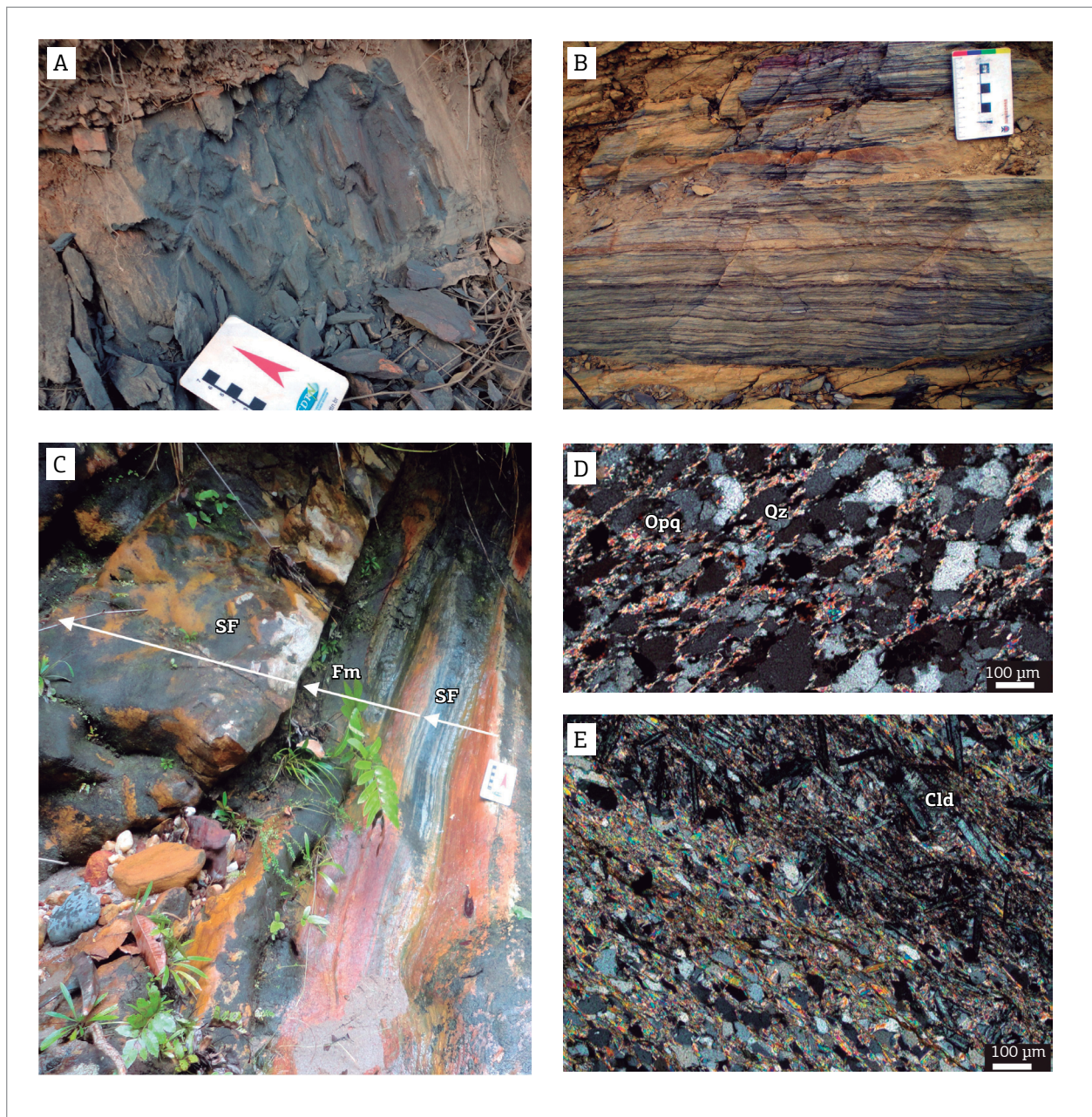
Figure 5. Lithofacies from the Canatiba Formation (A) Massive mudstone (Fm lithofacies); (B) Laminated sandstone and mudstone (SF lithofacies); (C) Turbiditic deposits with a thickening-upward facies succession; (D and E) Photomicrograph of the sandy and mudy portion (respectively) of rhythmite (lithofacies SF) with elongate quartz grains (Qz), opaque mineral (Opq) and chloritoid (Cld).

Facies association of Barrinha Member (FA3)

This association is well preserved from deformation and mainly consists of coarse-grained rocks with matrix- and clast-supported conglomerates (Gmm and Gcm lithofacies) and minor interbedded massive sandstone, and mudstone lenses (Sm and Fm lithofacies) in laterally discontinuous beds.

The Gcm lithofacies occurs subordinately and is characterized by massive clast-supported conglomerates, which range in thickness from 1 to 3 m. The clasts range from 4 to
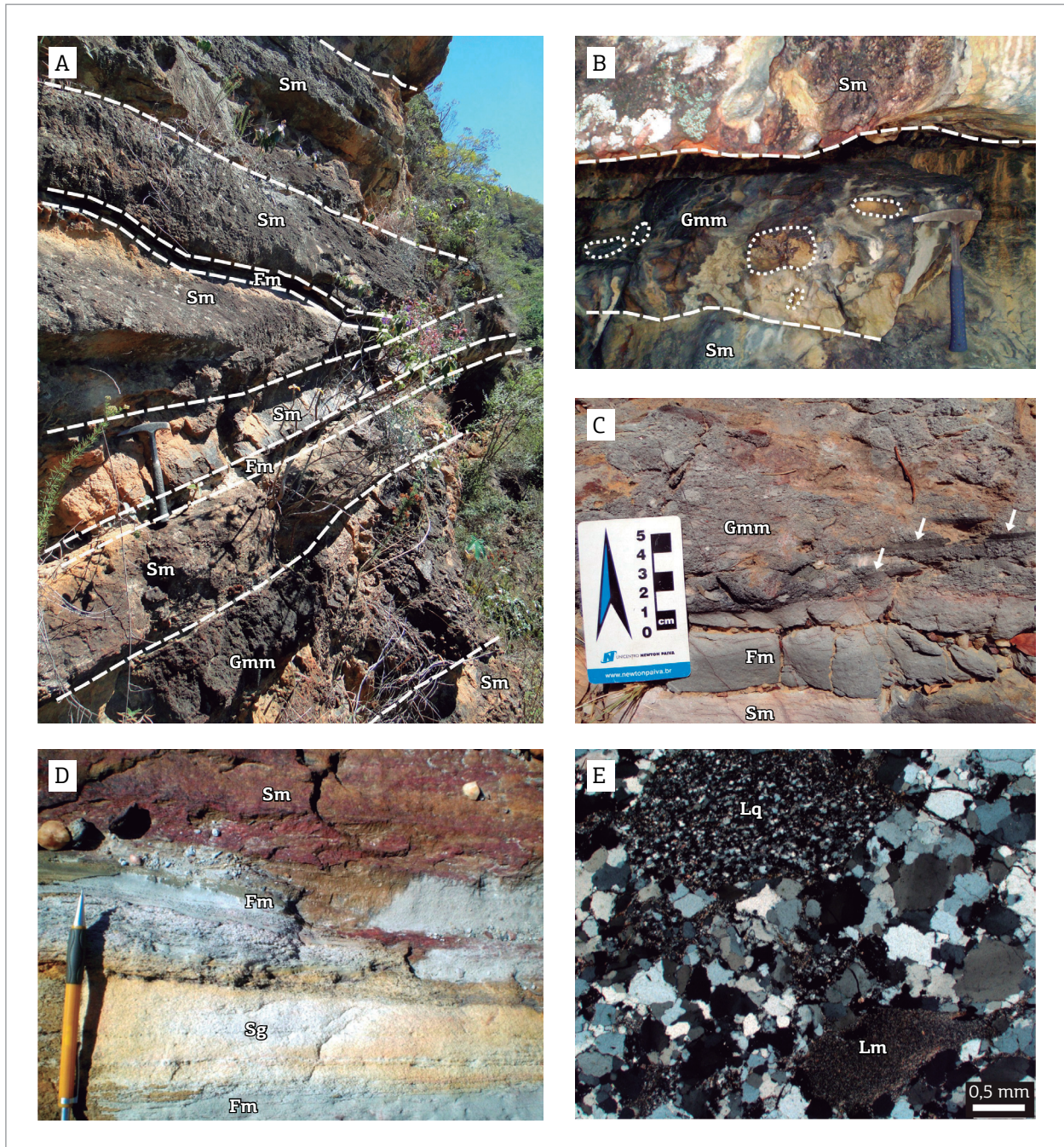
Figure 6. Lithofacies from the Rio Peixe Bravo Formation. (A) Medium to thick-bedded turbidite sandstones/pebbly sandstones with interbedded conglomerate and mudstone (Gmm and Fm lithofacies); (B) Lenticular conglomerate with sandstone clast (as marked) in massive sandstone showing erosional base(dashed line); (C) Massives sandstone and mudstone (Sm and Fm lithofacies) and polymict conglomerate (Gmm lithofacies); the arrows indicate to mudstone pebbles; (D) Medium-grained turbidites interbedded with mudstone lenses. (E) Photomicrograph of the Gmm lithofacies showing lithic fragment of quartzite (Lq) and mudstone (Lm).

40 cm in diameter and consist of quartz veins and sandstone, which is angular to rounded and poorly sorted (Fig. 7A). Sometimes, the Gcm lithofacies quickly transforms into the Gmm lithofacies.

Generally, the Gcm lithofacies shows no distinguishable bedding, which most likely represents megabeds. The conglomerate beds contain pebble- to cobble-grade, angular to rounded clasts in a disorganized framework (Fig. 7B). The clasts consist of sandstone, quartz-veins and mudstone and range from 5 to 70 cm in size (Fig. 7C). Scattered mudstone clasts locally occur in some beds (Fig. 7D). The matrix is poorly sorted, coarse to very coarse sandstone, which contains occasional granular sandstone and quartz. Lenses of mudstone and sandstone (Fm and Sm lithofacies) were observed to be interlayered in conglomerates at some locations. The contact with FA2 is transitional, as evidenced by a gradual decrease in the abundance of the gravel-sized clast population and an increase in sand in the matrix.

The poor sorting, disorganized framework of conglomerates and the absence of a primary structure suggest that FA3 was formed from extrabasinal debris flows (Lowe 1982, Zavala *et al.* 2011). The spatial distribution and presence of clast-supported conglomerates imply deposition by the channelized debris flows, which were possibly related to abrupt slopes (Postma *et al.* 1988). The very low mud content suggests a subaerial origin (Lowe 1982). The interlayers of massive mudstone and sandstone in the Gmm lithofacies indicate subaqueous conditions during the final depositional phase (Mutti 1992, Haughton *et al.* 2009).

U-Pb GEOCHRONOLOGY

Sample A1

Sample A1 is a rhythmite (SF lithofacies, Fig. 5B) from Canatiba Formation, which outcrops close to the Santo Onofre fault (Fig. 3). The zircon grains from this sample are rounded to sub-rounded, varying from 70 to 200 μm along the major axis. The CL images show that most of the
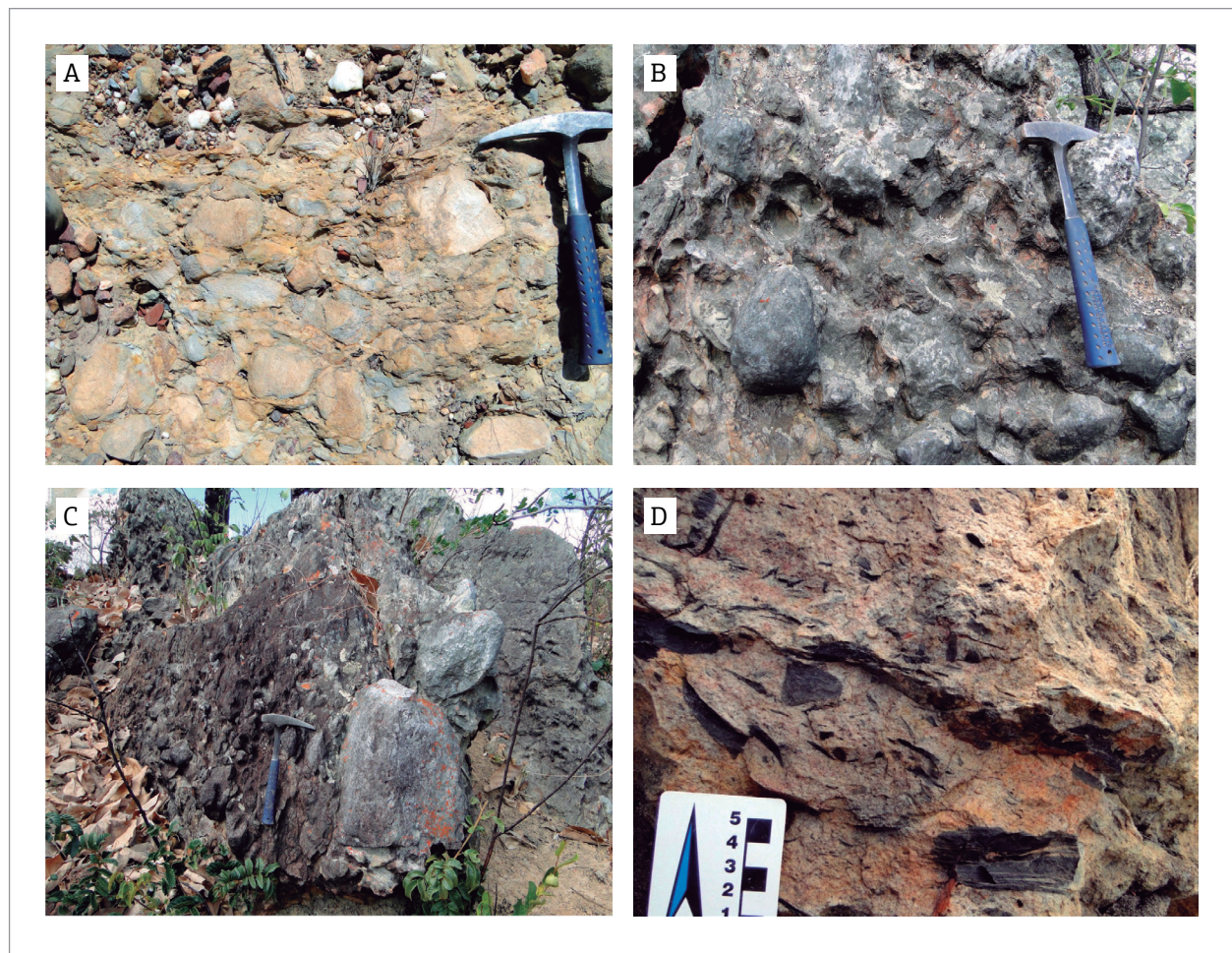
Figure 7. Lithofacies from the Barrinha Member. (A) Polymict clast-supported conglomerate (Gcm lithofacies). (B and C) Matrix-supported conglomerate (Gmm lithofacies); (D) Conglomerate with mudstone clast (Gmm lithofacies).

grains have oscillatory zoning (Fig. 8A). Some zircons do not present any internal structure or zoning.

Eighty-eight analyses on 85 zircon grains yielded ages from 3,111 to 914 Ma, with the following peaks: 2,930 Ma (n = 4), 2,170 Ma (n = 20), 1,791 Ma (n = 4), and 1,257 Ma (n = 5) (Fig. 8B). Most of the ages fall in the interval of 2,290 – 2,040 Ma (Tab. 2). Only three concordant ages were obtained within the youngest age mode. The weighted average of these three ages is 930 ± 33 Ma, which is interpreted as the maximum depositional age of Canatiba Formation.

Sample A2

Sample A2 is a sandstone (Sm lithofacies, Fig. 6A) from Rio Peixe Bravo Formation along the eastern border, close to the contact with the rocks from Barrinha Member (Fig. 3). Most of the zircon grains were translucent, ranging in color from white to brown, and varied from 100 to 250 μm along the major axis (Fig. 9A). The zircon grains had different shapes (sub-rounded, subhedral and prismatic). Broken fragments were common.

Seventy-three zircon age determinations on 70 zircon grains yielded ages from 2,838 to 857 Ma (Tab. 3, Fig. 9B). Several age peaks were defined for sample A2: 2,676 Ma (n = 4), 2,044 Ma (n = 4), 1,826 Ma (n = 7), 1,560 Ma (n = 4), and 1,051 Ma (n = 4). Concordant and similar values from two zircon grains (856 ± 6 and 873 ± 6 Ma) suggest a maximum depositional age for Rio Peixe Bravo Formation at c. 865 Ma.
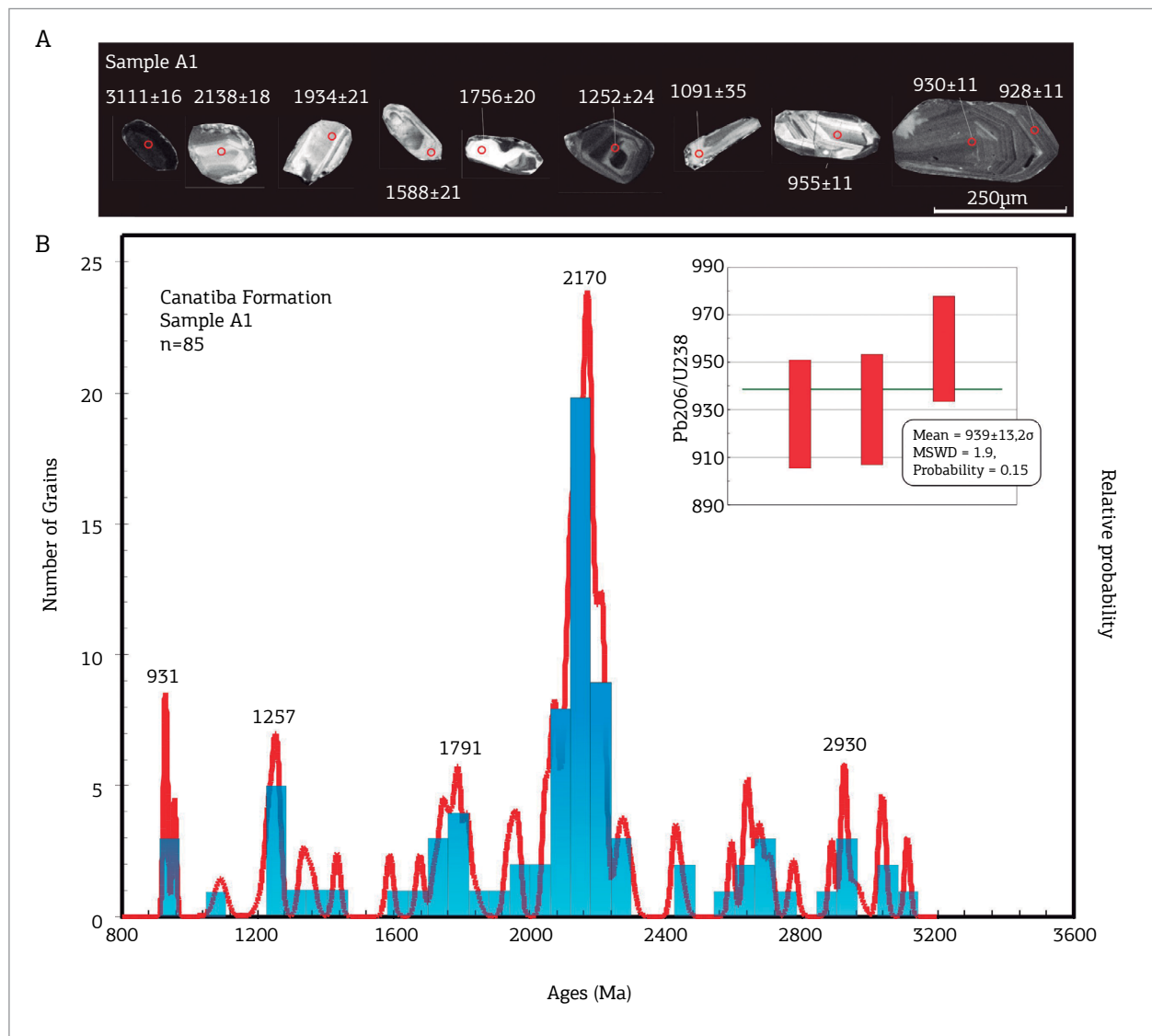
Figure 8. Sample A1 (Canatiba Formation) (A) CL images of selected detrital zircon grains representative of the calculated age. The red circles show the spot analysis. (B) Relative probability diagram for the detrital zircons.

Table 2. U-Pb (LA-ICP-MS) data for detrital zircon grains from sample A1 from the Canatiba Formation.

Spot	Ratios						Ages (Ma)						Conc.
	206/207	1σ	206/238	1σ	207/235	1σ	206/207	1σ	206/238	1σ	207/235	1σ	
1	0.0695	0.0010	0.1549	0.0020	1.485	0.023	914.6	29.46	928.2	11.39	924.1	9.21	99.56
2	0.0696	0.0009	0.1598	0.0020	1.534	0.021	916.5	25.23	955.8	11.1	943.9	8.4	98.74
3	0.0711	0.0010	0.1552	0.0021	1.521	0.024	960.4	29.36	930.2	11.67	939	9.53	100.94
4	0.0759	0.0013	0.1861	0.0028	1.945	0.036	1091.5	35	1100.2	15.24	1096.8	12.38	99.69
5	0.0811	0.0016	0.1970	0.0033	2.201	0.045	1224.2	39.3	1159.1	17.68	1181.4	14.18	101.89
6	0.0814	0.0009	0.2066	0.0025	2.319	0.029	1232	20.68	1210.5	13.23	1218.2	8.78	100.63
7	0.0823	0.0009	0.2164	0.0027	2.455	0.032	1252.2	21.89	1263	14.22	1258.9	9.47	99.67
8	0.0825	0.0010	0.2117	0.0028	2.406	0.035	1256.8	24.2	1237.8	15.05	1244.5	10.36	100.54
9	0.0825	0.0010	0.1994	0.0025	2.268	0.031	1257.4	23.32	1172.3	13.51	1202.4	9.55	102.50
10	0.0857	0.0010	0.2187	0.0028	2.584	0.035	1331.6	22.74	1274.7	14.99	1296	10.02	101.64
11	0.0868	0.0013	0.2340	0.0033	2.801	0.044	1356.9	28	1355.3	17.03	1355.8	11.74	100.04
12	0.0904	0.0010	0.2453	0.0030	3.057	0.039	1433.6	20.68	1414.1	15.44	1421.9	9.64	100.55
13	0.0981	0.0011	0.2730	0.0034	3.692	0.048	1588.7	21.26	1555.8	17.18	1569.7	10.37	100.89
14	0.1029	0.0012	0.2924	0.0037	4.148	0.054	1677.2	21.46	1653.5	18.35	1663.9	10.72	100.63
15	0.1055	0.0014	0.3020	0.0039	4.393	0.061	1723.8	23.73	1701	19.18	1711.1	11.39	100.59
16	0.1067	0.0011	0.3131	0.0038	4.604	0.056	1743.3	18.5	1755.8	18.47	1750	10.17	99.67
17	0.1074	0.0012	0.3087	0.0036	4.573	0.056	1756.4	20.95	1734.5	17.64	1744.4	10.29	100.57
18	0.1084	0.0012	0.3207	0.0040	4.792	0.061	1772.3	20.14	1793.2	19.28	1783.5	10.72	99.46
19	0.1093	0.0011	0.3132	0.0038	4.719	0.058	1787.5	18.92	1756.5	18.74	1770.7	10.38	100.80
20	0.1096	0.0012	0.3219	0.0039	4.866	0.060	1793.3	19.21	1799.2	18.86	1796.5	10.35	99.85
21	0.1110	0.0011	0.3196	0.0038	4.889	0.059	1815.2	17.69	1787.8	18.61	1800.4	10.11	100.70
22	0.1120	0.0022	0.3253	0.0054	5.020	0.096	1831.7	34.89	1815.4	26.35	1822.7	16.16	100.40
23	0.1186	0.0014	0.3456	0.0045	5.647	0.078	1934.7	20.88	1913.4	21.69	1923.3	11.98	100.51
24	0.1197	0.0012	0.3626	0.0043	5.985	0.074	1952.4	18.45	1994.3	20.53	1973.6	10.73	98.95
25	0.1204	0.0020	0.3120	0.0047	5.179	0.088	1962.8	29.6	1750.5	23.13	1849.2	14.52	105.34
26	0.1208	0.0012	0.3608	0.0044	6.007	0.073	1967.5	17.96	1986	20.69	1976.9	10.61	99.54
27	0.1261	0.0013	0.3849	0.0046	6.691	0.081	2044.2	17.64	2099	21.45	2071.4	10.64	98.67
28	0.1268	0.0016	0.3787	0.0046	6.620	0.085	2054.2	21.61	2070.2	21.62	2062	11.33	99.60
29	0.1280	0.0012	0.3810	0.0045	6.722	0.079	2070.1	17.01	2081.1	20.97	2075.5	10.43	99.73
30	0.1282	0.0016	0.3866	0.0052	6.832	0.095	2073.3	21.59	2107.1	23.94	2089.9	12.33	99.18
31	0.1284	0.0030	0.3793	0.0072	6.707	0.149	2076.1	40.17	2072.9	33.54	2073.5	19.59	100.03
32	0.1289	0.0013	0.3893	0.0046	6.920	0.083	2083.4	17.34	2119.5	21.48	2101.2	10.6	99.13
33	0.1303	0.0013	0.3861	0.0046	6.932	0.083	2101.4	17.42	2104.5	21.3	2102.8	10.67	99.92
34	0.1310	0.0015	0.3877	0.0049	7.001	0.090	2110.9	19.8	2112.3	22.8	2111.6	11.45	99.97
35	0.1312	0.0014	0.3940	0.0048	7.125	0.088	2113.7	18.3	2141.4	22.03	2127.2	11.03	99.33
36	0.1316	0.0016	0.3943	0.0052	7.155	0.098	2119.6	20.91	2142.9	24.1	2130.9	12.26	99.44
37	0.1317	0.0013	0.3877	0.0047	7.041	0.086	2121.3	17.25	2112	21.84	2116.6	10.87	100.22
38	0.1322	0.0015	0.3831	0.0045	6.980	0.086	2127	19.7	2090.8	21.09	2108.9	10.92	100.86
39	0.1325	0.0016	0.3921	0.0052	7.163	0.100	2131.8	20.55	2132.5	24.15	2131.9	12.41	99.97
40	0.1329	0.0014	0.3976	0.0049	7.283	0.091	2136.1	18.58	2158	22.54	2146.7	11.13	99.47
41	0.1329	0.0029	0.3761	0.0067	6.892	0.146	2137.2	37.79	2058.1	31.39	2097.6	18.75	101.88
42	0.1330	0.0013	0.3967	0.0047	7.273	0.086	2137.9	17.13	2153.6	21.75	2145.5	10.62	99.62
43	0.1330	0.0014	0.3991	0.0049	7.321	0.089	2138.3	18	2165.1	22.34	2151.4	10.91	99.36
44	0.1336	0.0014	0.3919	0.0048	7.220	0.089	2146.3	18.44	2131.4	22.28	2139	11.05	100.36

Continue...

Table 2. Continuation.

Spot	Ratios						Ages (Ma)						Conc.
	206/ 207	1σ	206/ 238	1σ	207/ 235	1σ	206/ 207	1σ	206/ 238	1σ	207/ 235	1σ	
45	0.1340	0.0014	0.3899	0.0049	7.204	0.092	2151	18.34	2122.5	22.88	2136.9	11.43	100.67
46	0.1343	0.0014	0.4026	0.0051	7.456	0.095	2155.2	18.46	2181.2	23.38	2167.7	11.46	99.38
47	0.1345	0.0019	0.3921	0.0054	7.267	0.107	2157.3	24.3	2132.4	24.89	2144.8	13.17	100.58
48	0.1345	0.0017	0.4052	0.0055	7.514	0.106	2157.5	21.53	2193	25.22	2174.7	12.61	99.16
49	0.1351	0.0014	0.4068	0.0050	7.576	0.093	2165	17.82	2200.4	22.67	2182.1	10.98	99.16
50	0.1351	0.0013	0.4001	0.0045	7.453	0.085	2165.3	17.18	2169.5	20.77	2167.3	10.18	99.90
51	0.1353	0.0014	0.4037	0.0049	7.533	0.091	2168.1	17.51	2186.2	22.27	2176.9	10.8	99.57
52	0.1355	0.0017	0.3977	0.0056	7.429	0.108	2170.6	22.23	2158.4	25.81	2164.5	13.03	100.28
53	0.1357	0.0015	0.4044	0.0049	7.563	0.096	2172.7	19.65	2189.2	22.62	2180.5	11.35	99.60
54	0.1358	0.0014	0.4059	0.0050	7.599	0.095	2174.5	18.09	2195.9	22.94	2184.8	11.21	99.49
55	0.1360	0.0014	0.3982	0.0049	7.464	0.093	2176.7	17.33	2160.5	22.71	2168.7	11.13	100.38
56	0.1362	0.0013	0.4044	0.0046	7.593	0.088	2179.6	16.83	2189	21.24	2184.1	10.35	99.78
57	0.1366	0.0016	0.3987	0.0055	7.508	0.106	2184.6	20.1	2163	25.45	2174	12.64	100.51
58	0.1369	0.0015	0.4059	0.0053	7.663	0.101	2188.9	18.46	2196.1	24.19	2192.3	11.8	99.83
59	0.1377	0.0019	0.4009	0.0059	7.610	0.116	2198.5	23.39	2173.2	27.1	2186.1	13.73	100.59
60	0.1379	0.0021	0.3940	0.0058	7.486	0.119	2200.6	26.4	2141.1	27.01	2171.3	14.2	101.39
61	0.1381	0.0030	0.3666	0.0066	6.971	0.146	2203.2	37.23	2013.5	30.95	2107.8	18.6	104.47
62	0.1381	0.0015	0.4062	0.0051	7.734	0.098	2203.6	19.07	2197.4	23.33	2200.6	11.41	100.15
63	0.1383	0.0025	0.4044	0.0067	7.703	0.144	2206.4	30.87	2189.3	30.58	2197	16.85	100.35
64	0.1390	0.0014	0.4047	0.0046	7.757	0.089	2215.1	17.3	2190.5	21.29	2203.2	10.38	100.58
65	0.1392	0.0015	0.4072	0.0050	7.815	0.097	2217	17.98	2202.3	23.06	2209.9	11.18	100.34
66	0.1397	0.0020	0.4097	0.0062	7.886	0.126	2223.1	24.85	2213.4	28.27	2218.1	14.45	100.21
67	0.1427	0.0019	0.4069	0.0058	8.001	0.119	2259.8	22.68	2200.7	26.46	2231.2	13.42	101.37
68	0.1441	0.0018	0.4229	0.0060	8.398	0.126	2276.8	21.85	2273.8	27.09	2274.9	13.65	100.05
69	0.1456	0.0023	0.4195	0.0063	8.416	0.142	2295	27.2	2258	28.72	2276.9	15.33	100.83
70	0.1573	0.0018	0.4524	0.0059	9.805	0.135	2426.4	19.73	2406.1	26.2	2416.7	12.64	100.44
71	0.1588	0.0025	0.4611	0.0069	10.088	0.175	2443.1	26.87	2444.6	30.6	2442.9	16.03	99.93
72	0.1737	0.0018	0.4945	0.0060	11.844	0.145	2594	17.46	2590	26.01	2592.2	11.47	100.08
73	0.1781	0.0019	0.5054	0.0061	12.410	0.153	2635.6	17.9	2636.8	25.99	2635.9	11.61	99.97
74	0.1792	0.0022	0.5089	0.0070	12.567	0.181	2645	20.42	2652	29.97	2647.8	13.58	99.84
75	0.1812	0.0042	0.4710	0.0088	11.755	0.262	2664.2	37.71	2487.8	38.34	2585	20.82	103.76
76	0.1827	0.0023	0.5152	0.0070	12.978	0.181	2677.8	20.57	2678.9	29.93	2678.1	13.15	99.97
77	0.1860	0.0026	0.5192	0.0073	13.312	0.205	2707.2	22.61	2695.9	30.93	2702	14.57	100.23
78	0.1940	0.0028	0.5384	0.0084	14.396	0.229	2776.3	23.22	2776.8	34.99	2776.1	15.13	99.97
79	0.2073	0.0040	0.5094	0.0088	14.551	0.278	2884.2	31.07	2653.9	37.46	2786.3	18.14	104.75
80	0.2079	0.0022	0.5633	0.0065	16.143	0.191	2888.9	17.09	2880.3	26.84	2885.3	11.3	100.17
81	0.2122	0.0023	0.5715	0.0067	16.715	0.197	2922.1	17.1	2913.9	27.44	2918.6	11.27	100.16
82	0.2129	0.0023	0.5771	0.0074	16.938	0.221	2927.8	17.58	2936.9	30.33	2931.3	12.52	99.81
83	0.2167	0.0052	0.5660	0.0116	16.829	0.404	2956.4	38.1	2891.3	47.94	2925.2	23.02	101.16
84	0.2270	0.0026	0.6015	0.0078	18.825	0.251	3031.2	18.53	3036	31.48	3032.9	12.86	99.90
85	0.2286	0.0025	0.5978	0.0073	18.840	0.233	3042.5	17.28	3020.8	29.31	3033.7	11.92	100.43
86	0.2357	0.0024	0.6088	0.0082	19.780	0.267	3091.1	16.43	3065.2	33.02	3080.6	13.03	100.50
87	0.2373	0.0053	0.5196	0.0094	16.919	0.390	3101.7	35.4	2697.3	39.87	2930.3	22.12	107.95
88	0.2387	0.0025	0.6194	0.0071	20.381	0.235	3111.1	16.61	3107.6	28.24	3109.6	11.18	100.06

DISCUSSION

Tectonics and basin-fill history

Although the original structural and stratigraphic record of the studied area have been modified by tectonic inversion (shortening, at least 35%), we can discuss some aspects regarding the tectonics and sedimentation of the remaining basin-fill succession of Santo Onofre Group. Schematic geological sections are presented in Figure 10, which shows the basin-fill history of the Santo Onofre paleo-basin. Some assumptions here must be tested in future works.

As previously shown, the study area contains Sítio Novo and Santo Onofre Groups, which represent two distinct basin-fill sequences (Fig. 10A and 10B). Beyond the contact angle between them (more than 40°), the sequence boundary between the facies successions of both units is marked by an abrupt shift in sedimentary facies. This shift is from shallow-marine facies associations to deep-water, hemipelagic and turbidite facies associations. These same relationships were found by Danderfer (2000) in northern Espinhaço for both lithostratigraphic units, suggesting a first-order regional tectonic control on the basin's formation and the sediment accumulation of Santo Onofre Group. In northern Espinhaço, Sítio Novo Group is interpreted as a rift fill-succession that preceded the deposition of Santo Onofre Group (Schobbenhaus 1996, Danderfer & Dardenne 2002). However, whether Sítio Novo and Santo Onofre Groups represent basin-fill sequences of distinct events or superposed rifting phases of a single event of crustal extension is still an open question, as is the hiatus between both groups.

The facies sedimentary pattern and the entire stratigraphic architecture of Santo Onofre Group suggest a sudden rise in
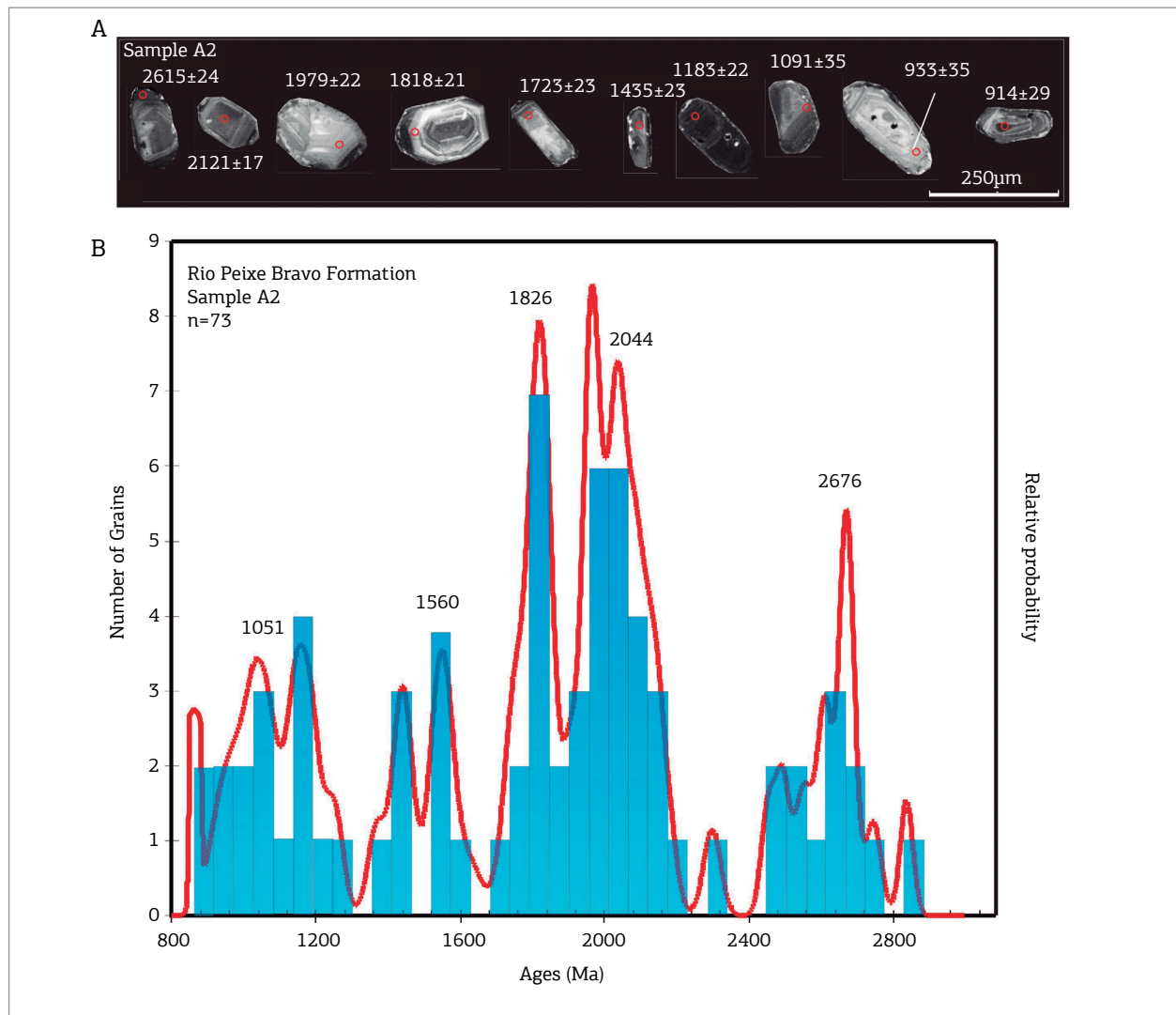
Figure 9. Sample A2 (Rio Peixe Bravo Formation) (A) CL images of selected detrital zircon grains representative of the calculated age. The red circles show the spot analysis. (B) Relative probability diagram for the detrital zircons.

Table 3. U-Pb (LA-ICP-MS) data for detrital zircon grains from sample A2 from the Rio Peixe Bravo Formation.

Spot	Ratios						Ages (Ma)						Conc.
	206/ 207	1σ	206/ 238	1σ	207/ 235	1σ	206/ 207	1σ	206/ 238	1σ	207/ 235	1σ	
1	0.06765	0.0009	0.142	0.001	1.324	0.013	857.85	26.24	855.8	5.58	856.3	5.65	100.1
2	0.06773	0.001	0.145	0.0011	1.3541	0.016	860.303	30.14	873	6.11	869.3	6.98	99.58
3	0.07016	0.0012	0.1593	0.0014	1.5405	0.023	933.039	35.69	952.7	7.67	946.7	9.38	99.37
4	0.07114	0.0015	0.1482	0.0014	1.4531	0.027	961.439	42.11	890.8	7.94	911.2	11.1	102.3
5	0.07198	0.0015	0.152	0.0015	1.5086	0.029	985.375	42.74	912.3	8.33	933.9	11.6	102.4
6	0.07301	0.0013	0.1461	0.0013	1.4703	0.023	1014.23	36.52	879.1	7.2	918.2	9.5	104.4
7	0.07363	0.001	0.1499	0.0011	1.5216	0.017	1031.34	27.31	900.5	6.16	939.1	6.72	104.3
8	0.07445	0.0023	0.173	0.0023	1.7754	0.051	1053.69	61.37	1028.5	12.43	1036.5	18.6	100.8
9	0.07466	0.0011	0.1733	0.0013	1.7837	0.021	1059.36	28.87	1030.5	7.11	1039.5	7.49	100.9
10	0.07556	0.0011	0.1522	0.0012	1.585	0.018	1083.44	28.17	913.1	6.56	964.3	7.19	105.6
11	0.07743	0.001	0.2044	0.0014	2.182	0.02	1132.29	24.49	1199.1	7.63	1175.3	6.52	98.02
12	0.07802	0.0009	0.1968	0.0013	2.1164	0.017	1147.38	22.27	1158	7.14	1154.2	5.57	99.67
13	0.07893	0.0012	0.2049	0.0017	2.2292	0.028	1170.38	29.08	1201.5	8.81	1190.3	8.65	99.07
14	0.07945	0.0009	0.2084	0.0014	2.2829	0.019	1183.37	22.45	1220.5	7.53	1207	5.83	98.89
15	0.08052	0.0014	0.2107	0.0019	2.3387	0.034	1209.75	33.3	1232.4	9.87	1224.1	10.5	99.33
16	0.08231	0.001	0.2063	0.0015	2.3404	0.022	1252.9	24.06	1208.9	7.93	1224.6	6.82	101.3
17	0.08729	0.0011	0.24	0.0018	2.8876	0.028	1366.9	24.2	1386.6	9.08	1378.7	7.38	99.43
18	0.09004	0.0014	0.2556	0.0021	3.1724	0.04	1426.38	28.69	1467.1	10.88	1450.5	9.76	98.87
19	0.09048	0.0011	0.246	0.0017	3.0677	0.028	1435.68	23.15	1417.6	8.92	1424.7	7.03	100.5
20	0.09125	0.0012	0.2533	0.0018	3.1866	0.032	1451.83	24.35	1455.7	9.44	1453.9	7.68	99.88
21	0.0947	0.0018	0.2668	0.0026	3.4827	0.058	1522.11	35.52	1524.7	13.17	1523.3	13.2	99.91
22	0.09526	0.0011	0.2726	0.0019	3.5793	0.031	1533.22	21.97	1553.9	9.82	1544.9	6.97	99.42
23	0.09662	0.0012	0.2707	0.0019	3.6058	0.034	1559.86	23.3	1544.5	9.51	1550.8	7.44	100.4
24	0.09684	0.0014	0.2641	0.0022	3.5252	0.043	1564.12	27.64	1510.6	10.99	1532.9	9.67	101.5
25	0.09987	0.0021	0.2649	0.0027	3.6444	0.066	1621.66	37.79	1514.6	13.88	1559.3	14.3	103
26	0.1057	0.0014	0.291	0.0023	4.2401	0.045	1726.52	24.45	1646.7	11.22	1681.8	8.73	102.1
27	0.10717	0.0012	0.3246	0.0023	4.7958	0.04	1751.84	20.72	1812.3	11.17	1784.2	7.05	98.45
28	0.10794	0.0015	0.2619	0.0019	3.8953	0.042	1764.93	25.23	1499.4	9.75	1612.7	8.73	107.6
29	0.10978	0.0013	0.3299	0.0023	4.992	0.045	1795.76	21.93	1837.8	11.21	1818	7.64	98.92
30	0.11008	0.0014	0.3246	0.0025	4.9257	0.049	1800.73	22.98	1812.2	12.03	1806.7	8.36	99.7
31	0.11029	0.0014	0.3293	0.0025	5.0057	0.051	1804.19	23.34	1834.7	12.09	1820.3	8.54	99.22
32	0.11114	0.0013	0.3161	0.0022	4.8426	0.043	1818.14	21.7	1770.6	10.94	1792.3	7.54	101.2
33	0.11149	0.0014	0.3379	0.0026	5.1937	0.052	1823.85	22.62	1876.6	12.68	1851.6	8.52	98.67
34	0.11221	0.0013	0.3328	0.0023	5.1486	0.044	1835.51	21.23	1852.1	11.01	1844.2	7.3	99.57
35	0.11244	0.0013	0.3315	0.0022	5.138	0.042	1839.22	20.7	1845.6	10.84	1842.4	7.02	99.83
36	0.11281	0.0023	0.3309	0.0037	5.1473	0.093	1845.17	36.21	1842.9	17.76	1843.9	15.3	100.1

Continue...

Table 3. Continuation.

Spot	Ratios						Ages (Ma)						Conc.
	206/ 207	1σ	206/ 238	1σ	207/ 235	1σ	206/ 207	1σ	206/ 238	1σ	207/ 235	1σ	
37	0.11376	0.0023	0.3404	0.0037	5.3383	0.095	1860.33	35.92	1888.4	17.56	1875	15.1	99.29
38	0.11695	0.0014	0.3567	0.0026	5.7499	0.049	1910.12	20.63	1966.4	12.13	1938.9	7.4	98.6
39	0.11718	0.0033	0.331	0.0041	5.3292	0.136	1913.65	49.94	1843.1	19.64	1873.6	21.9	101.7
40	0.11964	0.0014	0.36	0.0024	5.9357	0.047	1950.85	20	1982.1	11.33	1966.5	6.89	99.21
41	0.12015	0.0013	0.357	0.0024	5.9128	0.046	1958.45	19.56	1968	11.55	1963.1	6.76	99.75
42	0.12029	0.0015	0.3604	0.0026	5.9763	0.054	1960.53	21.25	1984.2	12.38	1972.4	7.81	99.41
43	0.12077	0.0016	0.3194	0.0024	5.3168	0.053	1967.63	22.79	1786.8	11.79	1871.6	8.53	104.7
44	0.12113	0.0016	0.3629	0.003	6.0603	0.067	1972.94	23.75	1995.9	14.11	1984.5	9.56	99.43
45	0.12154	0.0015	0.3679	0.0027	6.1635	0.059	1978.96	22.33	2019.5	12.9	1999.3	8.43	99
46	0.1217	0.0016	0.3663	0.0026	6.142	0.059	1981.3	22.74	2011.8	12.22	1996.2	8.39	99.22
47	0.1241	0.0016	0.3687	0.0028	6.3065	0.062	2015.99	22.41	2023.1	13.25	2019.4	8.61	99.82
48	0.12456	0.0014	0.3627	0.0025	6.227	0.051	2022.55	20.19	1994.7	11.72	2008.3	7.21	100.7
49	0.12503	0.0018	0.3483	0.0025	6.0006	0.067	2029.22	25.13	1926.7	11.99	1975.9	9.7	102.6
50	0.12547	0.0019	0.3641	0.0029	6.2924	0.076	2035.44	26.27	2001.3	13.81	2017.4	10.6	100.8
51	0.12602	0.0014	0.3722	0.0025	6.466	0.05	2043.17	19.36	2039.9	11.75	2041.3	6.79	100.1
52	0.1261	0.0015	0.3774	0.0027	6.5609	0.057	2044.3	20.56	2064.2	12.54	2054.1	7.64	99.51
53	0.12763	0.0015	0.3751	0.0026	6.5996	0.054	2065.58	19.94	2053.5	12.11	2059.3	7.21	100.3
54	0.12907	0.0015	0.377	0.0027	6.7066	0.057	2085.34	20.17	2062	12.48	2073.5	7.49	100.6
55	0.12919	0.0016	0.3757	0.0028	6.6896	0.064	2086.98	21.78	2055.9	13.33	2071.2	8.44	100.7
56	0.13035	0.0021	0.3852	0.0037	6.9208	0.096	2102.68	28.4	2100.5	17.16	2101.3	12.3	100
57	0.13172	0.002	0.3805	0.0034	6.9081	0.085	2121.02	25.87	2078.4	15.7	2099.7	10.9	101
58	0.13196	0.0018	0.3833	0.0031	6.9722	0.077	2124.21	23.92	2091.6	14.5	2107.9	9.75	100.8
59	0.13368	0.0017	0.3908	0.003	7.2019	0.07	2146.86	21.9	2126.6	13.71	2136.7	8.64	100.5
60	0.13594	0.0019	0.409	0.0033	7.6615	0.084	2176.1	24.13	2210.2	14.91	2192.1	9.88	99.18
61	0.14591	0.002	0.4029	0.0029	8.1008	0.087	2298.54	23.74	2182.4	13.1	2242.3	9.7	102.7
62	0.15986	0.0018	0.4646	0.0033	10.239	0.085	2454.18	19.26	2460	14.44	2456.6	7.71	99.86
63	0.16359	0.0018	0.3861	0.0026	8.7075	0.066	2493.11	18.15	2104.9	12.1	2307.9	6.92	109.6
64	0.16951	0.0051	0.4388	0.0057	10.215	0.28	2552.81	49.64	2345.3	25.65	2454.5	25.3	104.7
65	0.16953	0.0024	0.4646	0.0043	10.856	0.129	2553.01	23.54	2459.8	18.93	2510.8	11.1	102.1
66	0.17546	0.002	0.4714	0.0034	11.403	0.097	2610.42	19.13	2489.7	14.81	2556.6	7.95	102.7
67	0.17599	0.0025	0.4928	0.0045	11.953	0.147	2615.44	23.75	2582.9	19.58	2600.8	11.5	100.7
68	0.18131	0.002	0.5158	0.0036	12.891	0.104	2664.89	18.55	2681.4	15.18	2671.7	7.63	99.64
69	0.18156	0.002	0.4828	0.0032	12.082	0.096	2667.17	18.49	2539.3	14.07	2610.8	7.44	102.8
70	0.18217	0.0023	0.4894	0.004	12.289	0.121	2672.73	20.83	2568	17.11	2626.7	9.26	102.3
71	0.18343	0.002	0.5099	0.0036	12.893	0.103	2684.13	18.25	2656.2	15.46	2671.8	7.54	100.6
72	0.19037	0.0025	0.5069	0.0046	13.302	0.147	2745.36	21.77	2643.4	19.49	2701.3	10.4	102.2
73	0.20143	0.0022	0.5194	0.0035	14.42	0.113	2837.82	17.91	2696.5	14.94	2777.7	7.42	103

sea level, which was probably related to rapid tectonic subsidence (Jonhson *et al.* 2001, Prélat *et al.* 2009), explaining the shift in facies in Sítio Novo Group and the change to predominantly clastic sedimentation (shallow water to deep water). Danderfer (2000) interpreted the development of the accommodation space of the Santo Onofre paleo-basin under dextral transtractive tectonics based on structural evidence and the stratigraphic characteristics, with the east-dipping Muquém fault corresponding to the master fault in northern Espinhaço. According to this author, the Santo Onofre fault would correspond to the master fault of the Sítio Novo paleo-rift, which was reactivated during the Santo Onofre basin's formation. Two regional half-grabens developed in relation to both faults during the Santo Onofre rifting episode.

Along the investigated segment, the stratigraphic architecture of Santo Onofre Group also suggests the development of half-graben geometry, although there is no structural evidence to confirm the extensional regime (pure or transtractive). In this sense, we interpret the paleo-slope of the hanging wall to the west against the east-dipping Santo Onofre fault. This fault has been interpreted as a normal fault, which was reactivated as a west-verging reverse fault during Neoproterozoic inversion tectonics (Bertoldo 1993, Schobbenhaus 1993, Danderfer 2000). The relationship of younger strata (Santo Onofre Group), which were thrusted over older strata to the west of the fault (Espinhaço Supergroup), would confirm this interpretation. The bedding of Sítio Novo Group, which dips to the west with higher dip angles than Santo Onofre, also
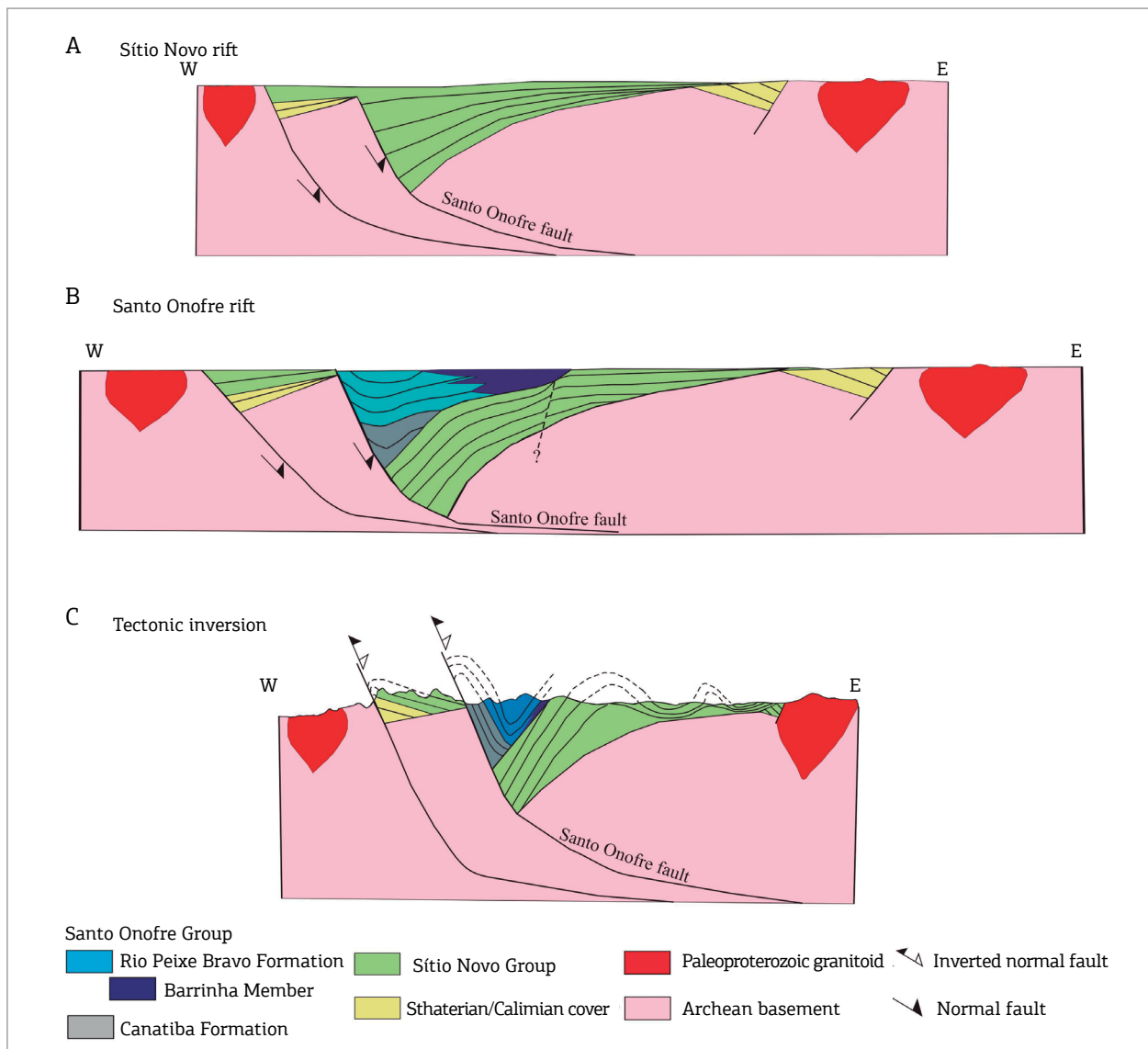
Figure 10. Sketch's showing the sedimentation and basin-fill history of the Santo Onofre basin, during (A) the open, deep-water lacustrine and/or marine phase and (B) the shallow to deep-water phase. In (C), a section showing the structural geometry from the inversion tectonics (constructed based on rules of structural balancing, respecting as much as possible the geological map and the integration of field data).

favors the tilting of the hanging wall to the west (Tinterri *et al.* 2017, Link 2003, Poyatos-Moré *et al.* 2016).

A stratigraphic problem arises when considering the Santo Onofre fault as the edge fault of the half-graben: no coarse siliciclastic sediment deposits were found near this fault, as expected in related depositional models (Link 2003, Noda & Toshimitsu 2009, Hubbard *et al.* 2010, Dixon *et al.* 2012). This fact was also observed along the northern Espinhaço (Dominguez 1993, Danderfer 2000).

Some assumptions may be presented to explain the absence of coarse-grained facies near the Santo Onofre fault. One hypothesis could be a basin inversion (thrusting, tight folding and uplift of the hanging wall), which caused the exhumation of the younger facies and their subsequent erosion; this process supposedly includes western deposits from Rio Peixe Bravo Formation, which are theoretically arranged next to the master fault. Another explanation is related to the minor local supply of materials from the transversal filling of the basin (Agirrezabala & Mondejar 1994, Tinterri *et al.* 2017) or the submersion of the footwall of the Santo Onofre fault, which did not expose rocks to erosion and sediment generation (Surlyk 1984). In this case, the axial supply from a source outside the study area would dominate the basin infill, as characterized by Danderfer (2000) in northern Espinhaço. In addition, source areas of siliciclastic detritus to the east are favored by the existence of conglomeratic deposits of Barrinha Member.

The sedimentary infilling of the half-graben in the Santo Onofre basin could be described in two phases: a sea-level highstand phase (Fig. 10B) and an upward, shallowing-water sedimentation phase (Fig. 10C). The narrow and restricted occurrence of carbonaceous mudstone facies that are interbedded with fine-grained turbidites from Canatiba Formation suggests the depocenter was located near and along the entire extension of the Santo Onofre fault, occurring probably directly on Sítio Novo Group (this contact is seen only in northern Espinhaço, Danderfer 2000). Therefore, the western portion of the half-graben, where the area of largest subsidence is expected to be located (Prélat *et al.* 2009, Link 2003, Noda & Toshimitsu 2009, Poyatos-Moré *et al.* 2016), suggests a greater ratio of accommodation for sedimentation during stagnant, poorly oxygenated deep water during the sea-level highstand phase. These conditions favored high biological activity, serving as a source of carbonaceous material (Canfield *et al.* 2007, Sato *et al.* 2015).

The highstand water conditions changed to the east, where the fine-grained facies of Canatiba Formation disappear. With time, the basin became progressively shallower, favoring the deposition of the coarsening-upward, sandstone-rich turbidite succession of Rio Peixe Bravo, as reported for Ridge Basin, in California (Link 2003); the same pattern of filling

occurred in northern Espinhaço, as recorded in Boqueirão Formation (Danderfer & Dardenne 2002). The abundance of fine-grained turbidites in the eastern portion matches the relatively distal position of a submarine fan and/or a relatively low slope that was associated with the hanging wall in asymmetric extensional basins (Reading & Richards 1994, Haughton 2001). In this sense, the filling of the basin itself, as indicated by the decrease in slope, could explain the gradual transition from the mudstone facies (deep water) association to the sandstone facies (relative shallower water). The presence of coarse-grained turbidites in the western portion of the half-graben can be associated with hyper-concentrated flows that transformed from originally extrabasinal debris flows (Haughton *et al.* 2009, Zavala *et al.* 2011). The conglomerates from Barrinha Member could be interpreted as local, gravel-rich submarine channel deposits originated from the east. The size and shape of the clasts in the conglomerate deposits suggest proximity to the source area. Otherwise, this deposit could be related to an antithetical fault along the eastern border of the Santo Onofre paleo-basin.

Relative timing of the Macaúbas and Santo Onofre rifts

As previously explained, the areas where Santo Onofre and Macaúbas Groups were defined are in distinct regions. The correlation between these units was originally proposed by Schobbenhaus (1996) and then by Danderfer (2000), who tracked some physical continuity between them along the northern portion of central and northern Espinhaço. According to Schobbenhaus (1996), the Santo Onofre rift originated as an arm of a triple junction related to the opening of the Macaúbas basin. However, the absence of absolute ages for both makes the correlation process debatable. The timing between both basin-fill successions and problems that are related to stratigraphic correlations could be better discussed in this study, considering the new data acquired in our studies, and compared to what has already been published for each unit in their respective type-areas.

The first point concerns the tectonic truncation between the Macaúbas and Santo Onofre basin-fill sequences. Approximately in the middle of central Espinhaço, the N-S stratigraphic trends of Santo Onofre and Sítio Novo Groups are truncated by the NE-SW stratigraphic trend of the glacial sequence of Nova Aurora Formation (Upper Macaúbas Group, Alkmim *et al.* 2017). This truncation is clearly marked by a magnetic analytical signal (Fig. 11). In map view, the contact between both successions is marked by Córrego do Buraco Shear Zone, with reverse movement verging to the NW, which placed the youngest unit over the oldest one (Lombello *et al.* 2014). These relationships suggest a normal fault that was inverted into reverse movement along the contact between Macaúbas

and Santo Onofre Groups, probably during Neoproterozoic contractional deformation. In this context, truncation could be interpreted as the master fault of the Macaúbas rift, which truncated the previous trend of the Santo Onofre rift.

The second point is related to the age spectra of U-Pb detrital zircons from the Macaúbas and Santo Onofre units, which are similar in some aspects. Archean to Neoproterozoic sources are predominant in both units (Babinski *et al.* 2012, Kuchenbecker *et al.* 2015). However, the youngest geochronological pattern found in Santo Onofre Group (< 900 Ma) has not yet been detected in the pre-glacial Lower Macaúbas Group. A relationship between Tonian-age spectra from detrital zircons in pre-glacial sequences and rift-related magmatism from c. 957 to 875 Ma has been proposed (Silva *et al.* 2008,
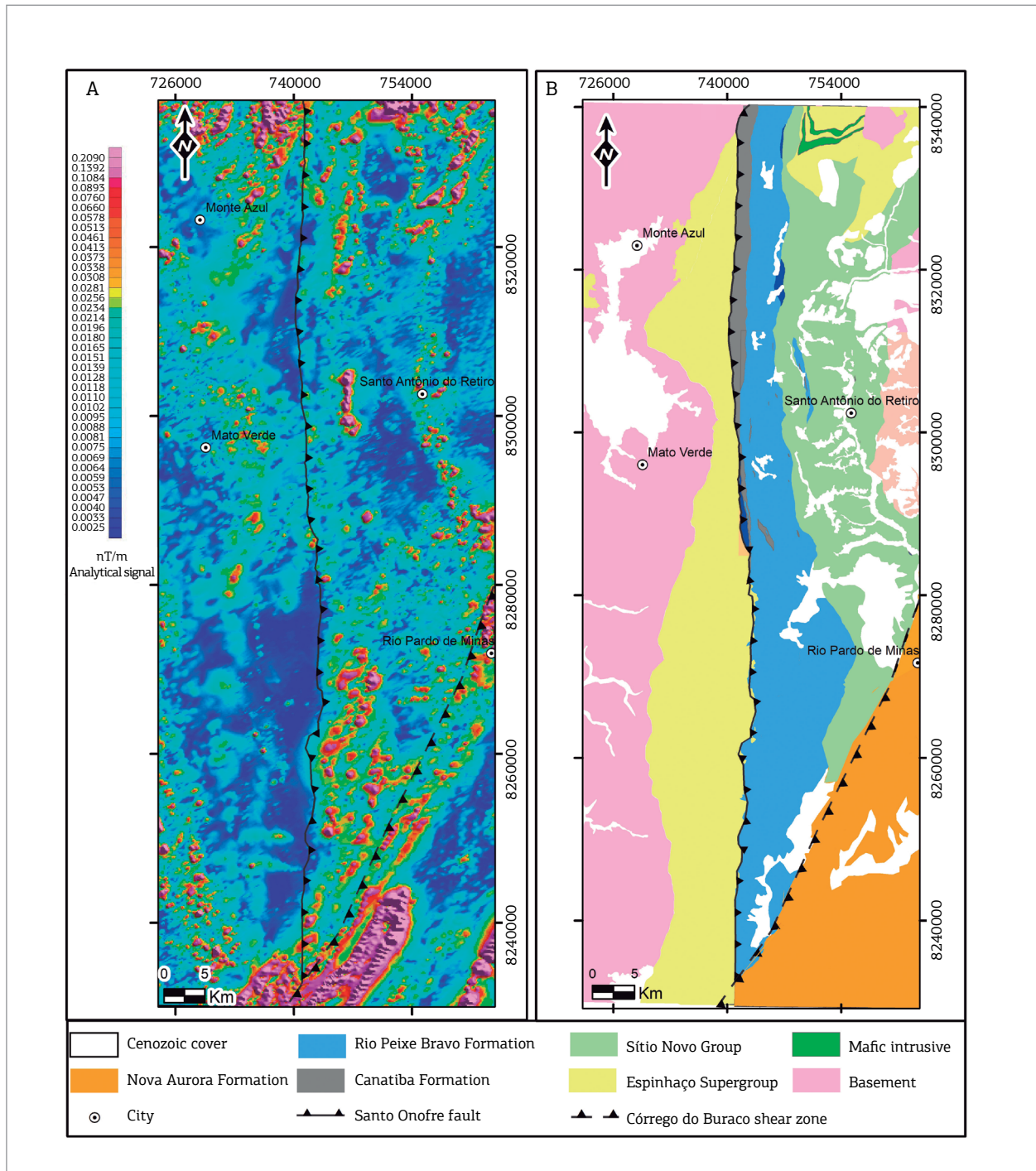
Figure 11. (A) Analytical signal map. (B) Simplified geologic map of the central Espinhaço region. Modified from Souza *et al.* (2003), Pinheiro *et al.* (2014), Lombello *et al.* (2014), Queiroz *et al.* (2014).

Castro 2014, Queiroga *et al.* 2012). Santo Onofre Group contains younger zircons, which are 828 Ma in northern Espinhaço (Sousa *et al.* 2014) and around 865 Ma in the study area. On the other hand, the glacial and post-glacial sequences that comprise Middle and Upper Macaúbas Groups (Alkmim *et al.* 2017), respectively, exhibit younger age patterns than the Santo Onofre succession, which is younger than 750 Ma (Kuchenbecher *et al.* 2015, Queiroga 2010).

The final issue concerns the sedimentary features (environments and depositional systems) which characterize the Macaúbas and Santo Onofre successions. The lower pre-glacial sequence of Macaúbas Group encloses a siliciclastic, continental to shallow-marine succession (Martins *et al.* 2008). Carbonaceous mudstones and thick turbidite successions are described only in Rio Peixe Bravo Formation (Viveiros *et al.* 1978, Noce *et al.* 1997), which are a fundamental component of Santo Onofre Group (Danderfer & Dardenne 2002) and suggest this unit was deposited under reducing conditions (Lash & Blood 2014). The sedimentation of the successions above Rio Peixe Bravo Formation was strongly influenced by glaciogenic processes (Noce *et al.* 1997, Pedrosa-Soares *et al.* 2011) without associated reducing conditions. In this case, the sedimentation of Santo Onofre Group preceded the glacial event, which supposedly occurred during Late Tonian (Shields 2016).

Accordingly, we interpret Santo Onofre and Macaúbas Groups to represent distinct basin-fill successions in terms of tectonic style, depositional setting, and environmental conditions. We interpret the Santo Onofre rifting to be younger than that for Sítio Novo Group (Danderfer & Dardenne 2002) and related formations from Lower Macaúbas Group (Alkmim *et al.* 2017), namely, Capelinha, Matão, Duas Barras and Domingas Formations. This rifting episode would have been a precursor stage of the glacial and post-glacial sequences from Middle and Upper Macaúbas Groups, which were related to the breakup and opening of the Macaúbas basin (Alkmim *et al.* 2017). The timing of these events requires better constraints.

Macaúbas Supergroup

According to Schobbenhaus (1993, 1996), Danderfer and Dardenne (2002), our results, and several works on Macaúbas Group (compiled in Alkmim *et al.* 2017), we propose a change in the rank of the "Macaúbas" stratigraphic unit from "group" to "supergroup", in order to accommodate the main unconformity-limited sequences with Tonian ages. Thus, Macaúbas Supergroup would be represented by Sítio Novo and Santo Onofre Groups, which occur along northern Espinhaço and the northern portion of central Espinhaço, and related units defined within the original Macaúbas Group in terms of its locality (Fig. 12).
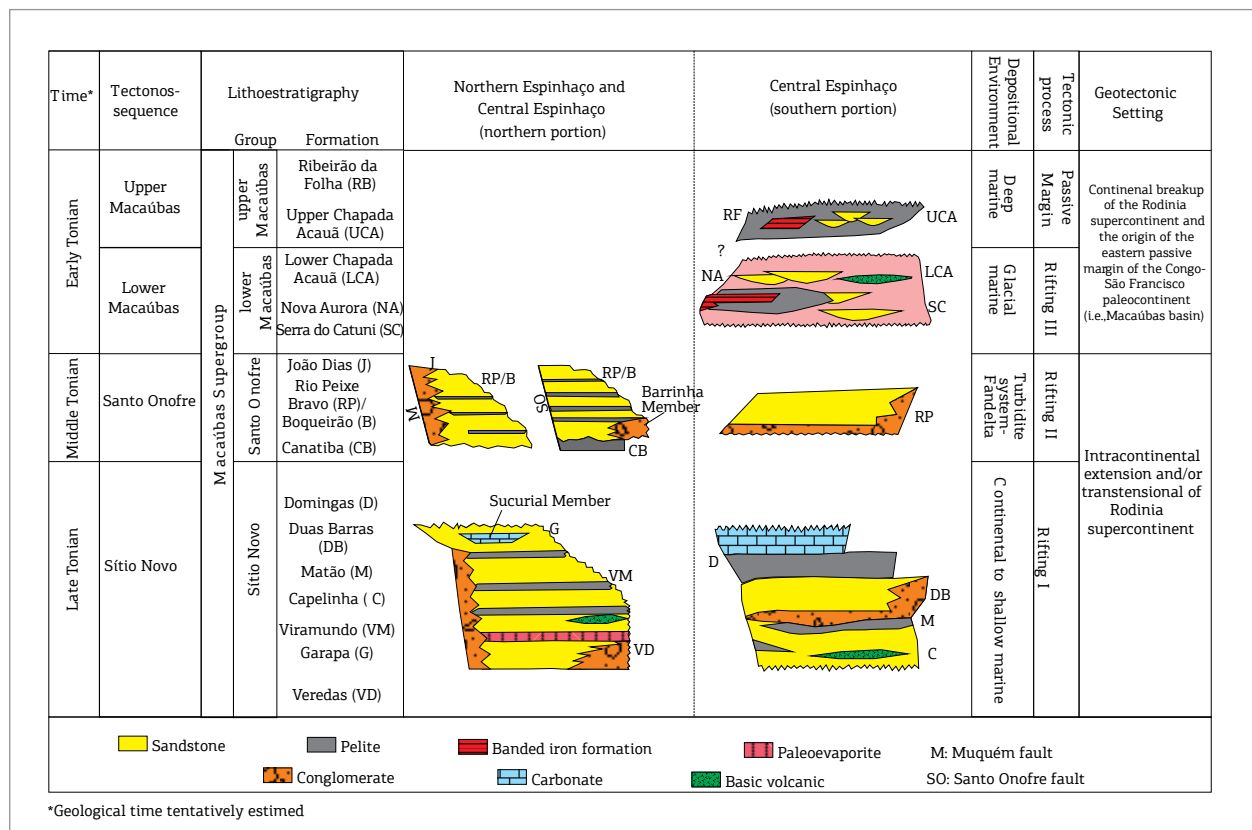
Figure 12. Stratigraphic framework for the Macaúbas Supergroup.

This redefinition makes the Tonian sequences easier to recognize, map, and extend throughout the Paramirim aulacogen and the Araçuaí belt, including non-glacial, glacial and post-glacial units, opening a new perspective to understand the geotectonic evolution of the Congo-São Francisco paleocontinent, as noted by Schobbenhaus (1993, 1996). Each sequence represents a distinct space-time phase of tectonic activity related to the rupturing of the Rodinia supercontinent (Fig. 13), and is a first-order tectono-stratigraphy sequence linked to different basin-forming tectonics (Danderfer & Dardenne 2002, Kuchenbecker *et al.* 2015). This redefinition also enables us to separate Tonian sequences from the Cryogenian to Ediacaran sequences of São Francisco Supergroup, whose geneses were associated with orogenic processes in foreland and synorogenic basins (Alkmim *et al.* 2017, Reis *et al.* 2017).
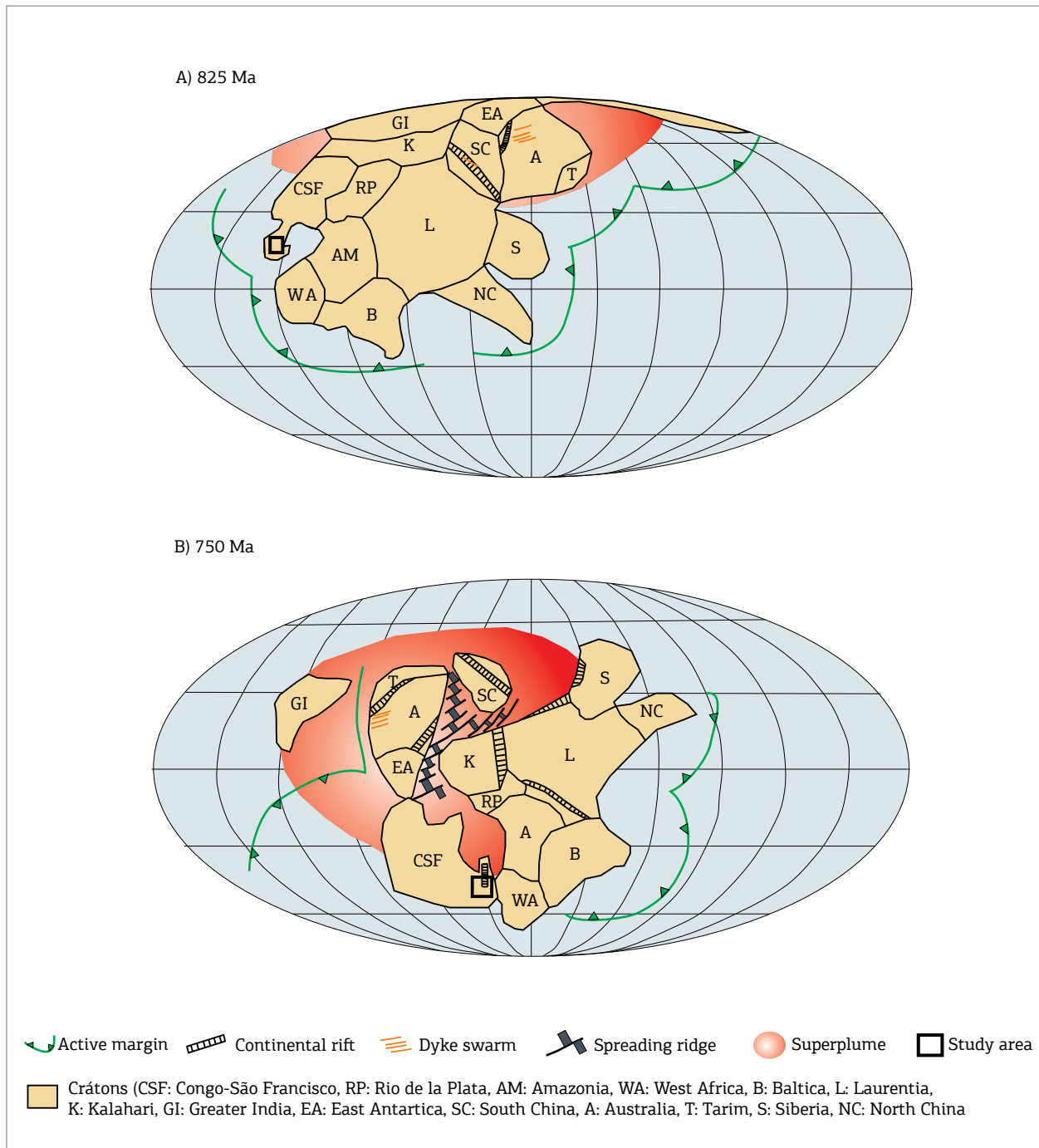
Figure 13. Cartoons to explain intracontinental rifting during the break-up of Rodinia, by Li *et al.* (2008). (A) Initial fragmentation related to Santo Onofre rift. (B) Final major break-up event related to Macaúbas rift.

Accordingly, Macaúbas Supergroup consists of four first-order tectono-sequences. The concept of tectono-sequence was introduced by Silva (1993) to define spatial and temporal arrangement of strata deposited during a specific tectonic phase.

1. Sítio Novo Tectono-sequence, which includes the formations from Sítio Novo Group and Capelinha, Matão, Duas Barras and Domingas Formations (in Lower Macaúbas Group, Alkmim *et al.* 2017). All the successions represent the first intracontinental rifting stage, with sedimentation dominated by continental to shallow-marine depositional systems (Danderfer & Dardenne 2002, Karfunkel & Karfunkel 1976, Noce *et al.* 1997, Martins *et al.* 2008, Leite 2013). The age of this tectono-sequence was constrained to 957 Ma according to syn-sedimentary magmatism ages (Castro 2014); the youngest U–Pb ages of detrital zircons produced maximum depositional ages of around 950 Ma (Martins *et al.* 2008, Babinski *et al.* 2012, Sousa *et al.* 2014).

2. Santo Onofre Tectono-sequence, which comprises the formations of Santo Onofre Group (Danderfer & Dardenne 2002), including Rio Peixe Bravo Formation, which was originally defined by Viveiros *et al.* (1978) and was observed in Lower Macaúbas Group by Alkmim *et al.* (2017). This sequence records a second intracontinental rifting stage, with predominantly turbidite sedimentation associated with fan-delta deposits (Danderfer & Dardenne, 2002). The youngest U–Pb ages of detrital zircons produced maximum depositional ages between 828 and 865 Ma (Sousa *et al.* 2014).

3. Lower Macaúbas tectono-sequence, which includes Jequitaí, Serra do Catuni, Nova Aurora and Lower Chapada Acauã Formations in Middle Macaúbas Group (Alkmim *et al.* 2017). This sequence was deposited in glaciomarine and glacio-terrestrial settings (Uhlein *et al.* 2007, Pedrosa-Soares *et al.* 2011), and was related to the last intracontinental rifting phase following the breakup of Rodinia. The youngest U–Pb ages of detrital zircons produced maximum depositional ages of around 935 Ma (Babinski *et al.* 2012, Kuchenbecker *et al.* 2015).

4. Upper Macaúbas tectono-sequence, which includes the post-glacial upper Chapada Acauã and Ribeirão da Folha Formations in Upper Macaúbas Group and records a transition to a passive-margin siliciclastic succession (Alkmim *et al.* 2017). The youngest U–Pb ages of detrital zircons produced maximum depositional ages of around 750 Ma (Kuchenbecker *et al.* 2015). However, ophiolite ages acquired by Queiroga *et al.* (2007) indicate the ocean basin related to the development of this passive margin extended into the Cryogenian.

CONCLUSIONS

Santo Onofre Group records the infill of a Tonian, extensional/transtractive basin developed along the northern and central Espinhaço regions and succeeded the Sítio Novo basin-fill succession. The following conclusions can be summarized from this unit in the northern region of central Espinhaço:

1. Santo Onofre Group was redefined and subdivided into two formations, namely, Canatiba and Rio Peixe Bravo Formations, which include Barrinha Member. Canatiba Formation predominantly comprises carbon-rich, massive and laminated mudstones related to deep-water sedimentation under reducing conditions. Rio Peixe Bravo Formation mainly consists of coarse to fine sandstone deposited through high- to low-density turbidity currents. Barrinha Member occurs locally, intertongues with turbidite beds or lies directly over Sítio Novo Group to the east, and comprises conglomerates with subordinate sandstones related to channelized debris flows.

2. The stratigraphic architecture suggests the development of a half-graben, where two stages were recognized during the filling of the basin:
   a. a sea-level highstand phase; and
   b. a shallowing-water sedimentation phase.

The first phase produced the deep-water deposits of Canatiba Formation in the western portion, where the depocenter was located near the Santo Onofre fault. During the second phase, the paleo-basin became progressively shallower, favoring the deposition of the sandy turbidites of Rio Peixe Bravo Formation.

3. The detrital zircon grains extracted from Santo Onofre Group mainly showed Archean and Paleoproterozoic ages, with a maximum depositional age given by the weighted averages of 930 ± 33 Ma and 856 Ma for Canatiba and Rio Peixe Bravo Formations, respectively.

4. To the south, the Santo Onofre fault and the N-S bedding trend of Santo Onofre and Sítio Novo Groups are truncated along a SE-dipping reverse fault zone, whose hanging wall consists of the glacial sequences of Nova Aurora Formation, with a NE-SW bedding trend. This fault is interpreted as an old inverted normal fault and may correspond to the edge of a relatively younger rifting episode, which was probably related to the last stage of the breakup of the Rodinia supercontinent.

5. Regional reevaluation suggests that the central and northern Espinhaço record three superposed Tonian rifting episodes, followed by the passive margin stage of the Macaúbas basin. The former contains the sedimentary successions of Sítio Novo Group and a portion of

Lower Macaúbas Group. The second rifting was recorded by the Santo Onofre basin-fill succession, including Rio Peixe Bravo Formation, which was originally positioned in Lower Macaúbas Group. The last rifting episode is related to Middle Macaúbas Group, whose succession was deposited under glaciogenic conditions. Upper Macaúbas Group corresponds to the transitional-passive margin sequence.

6. Our results and literature data led us to propose a change in the hierarchy of Macaúbas Group to a Supergroup, designating four unconformity-limited sequences of Tonian ages, including Sítio Novo, Santo Onofre, Lower and Upper tectono-sequences. Additional studies are necessary in order to better constrain the timing of these sequences.

ACKNOWLEDGEMENTS

REFERENCES

Agirrezabala L.M. & Mondejar G.J. 1994. A coarse grained turbidite system with morphotectonic control (Middle Albian, Ondarroa, northern Iberia). *Sedimentology,* **41**: 383407.

Alkmim F.F.; Brito Neves B.B.; Castro Alves J.A.1993. Arcabouço tectônico do Cráton do São Francisco - Uma Revisão. In: Dominguez, J.M.L. &Misi, A. (eds) *O Cráton do São Francisco.* Salvador, SBG/Núcleo BA/SE, SGM/BA. p. 45-62.

Alkmim F.F., Marshak S., Pedrosa-Soares A.C., Peres G.G., Cruz S.C. Whittington A. 2006. Kinematic Evolution of the Araçuaí–West Congo orogen in Brazil and Africa: Nutcracker tectonics during the Neoproterozoic assembly of Gondwana. *Precambrian Research,* **149**:43-64.

Alkmim F.F. & Martins-Neto M.A. 2012. Proterozoic first-order sedimentary sequences of the São Francisco craton, eastern Brazil. *Marine and Petroleum Geology,* **33**: 127-139.

Alkmim F.F., Kuchenbecker M., Reis H.L.S., Pedrosa-Soares A.C. 2017. The Araçuaí Belt. In: Heilbron M., Cordani U.G., Alkmim F.F. (eds.). *São Francisco Craton, Eastern Brazil: Tectonic Genealogy of a Miniature Continent, Brazil,* Springs, p. 255-276

Almeida F.F.M. 1977. O Cráton do São Francisco. *Revista Brasileira de Geociências,* **7**:349-364.

Babinski M., Pedrosa-Soares A.C., Trindade R.I.F., Martins M., Noce C.M., Liu D. 2012. Neoproterozoic glacial deposits from the Araçuaí orogen, Brazil: Age, provenance and correlations with the São Francisco Craton and West Congo belt. *Gondwana Research,* **21**:451-465.

Bertoldo A.L. 1993. *Comportamento estrutural dos supergrupos São Francisco e Espinhaço e do embasamento entre a serra do Espinhaço setentrional e as serras de Monte Alto (BA) e Central (MG).* MS Dissertation, Instituto de Geociências, Universidade Federal do Rio de Janeiro, Rio de Janeiro, 87p.

Bruni M.A.L., Almeida J.T., Bruni E.C. Folha Rio São Francisco (SC.23). 1976. *In: Carta geológica do Brasil ao Milionésimo.* Brasília: DNPM. 56p (Texto explicativo).

Canfield D.E., Poulton S.W., Narbonne G.M. 2007. Late-Neoproterozoic deep-ocean oxygenation and the rise of animal life. *Science,* **315**:949-952

Castro M.P. 2014. *Caracterização Geológica da Formação Capelinha como uma unidade basal do Grupo Macaúbas em sua área tipo, Minas Gerais.* MS Dissertation, Departamento de Geologia, Universidade Federal de Ouro Preto, Ouro Preto, 113p.

Cawood P.A., Strachan R.A., Pisarevsky S.A., Gladkochub D.P., Murphy J.B. 2016. Linking collisional and accretionary orogens during Rodinia assembly and breakup: Implications for models of supercontinent cycles. *Earth and Planetary Science Letters,* **449**:118-126.

Chemale Jr. F., Dussin I.A., Alkmim F.F., Martins M.S., Queiroga G., Armstrong R., Santos M.N. 2012. Unravelling a Proterozoic basin history trough detrital zircon geochronology: The case of the EspinhaçoSuperGroup, Minas Gerais, Brazil. *Gondwana Research,* **22**:200-206.

Chew D.M., Fallon N., Kennelly C., Crowley Q., Pointon M. 2010. Basic volcanism contemporaneous with the Sturtian glacial episode in NE Scotland. *Earth Environmental Science Transactions Royal Society Edinburgh,* **100**:399-415.

Cordani U.G., Fraga F.M., Reis N., Tassinari C.C.G., Brito-Neves B.B. 2010. On the origin and tectonic significance of the intra-plate events of Grenvillian-type age in South America: A discussion. *Journalof South American Earth Sciences,* **29**:143-159

Costa A.F.O. 2013. *Estratigrafia e tectônica da borda oeste do Espinhaço Central no extremo norte da Faixa Araçuaí.* MScDissertation, Departamento de Geologia/Escola de Minas, Universidade Federal de Ouro Preto, Ouro Preto, 170p.

Costa A.F.O., Danderfer A., Lana C. 2014. O registro do vulcanismo calimiano no Espinhaço Central (MG): caracterização petrofaciológica, geoquímica e geocronológica. *Revista Geociências,* **33**:119-135

Cruz S.C.P. & Alkmim F.F. 2006. The tectonic interaction between the Paramirim Aulacogen and the Araçuaí Belt, São Francisco Craton region, Eastern Brazil. *Anais da Academia Brasileira de Geociências,* **1**:151-173p.

Cruz S.C.P. & Alkmim F.F. 2017. The ParamirimAulacogen In: Heilbron M., Cordani U.G., Alkmim F.F. (eds.). *São Francisco Craton, Eastern Brazil: Tectonic Genealogy of a Miniature Continent, Brazil,* Springs, p. 97-115.

Danderfer A. 2000. *Geologia Sedimentar e Evolução Tectônica do Espinhaço Setentrional, Estado da Bahia.* PhDThesis, Universidade de Brasília, Brasília, 498p.

Danderfer A. & Dardenne M.A. 2002. Tectonoestratigrafia da bacia Espinhaço na porção centro-norte do cráton do São Francisco: registro de uma evolução poli-histórica descontínua. *Revista Brasileira de Geociências,* **32**(4):449-460.

Danderfer A., Lana C.C., Nalini H.A., Costa A.F.O. 2015. Constraints on the Statherian evolution of the intraplate rifting in a Paleo-Mesoproterozoic paleocontinent: New stratigraphic and geochronology record from the eastern São Francisco craton. *Gondwana Research,* **28**:668-688.

Danderfer A., Waele B.D., Pedreira A.J., Nalini H.A. 2009. New geochronological constraints on the geological evolution of Espinhaço basin within the São Francisco Craton – Brazil. *Precambrian Research*, **170**:116-128

Dixon J.F., Steel RJ., Andolariu C. 2012. Shelf-edge delta regime as a predictor of deep-water deposition: *Journal of Sedimentary Research*, **86**:681-687.

Dominguez J.M.L. 1993. As coberturas do Cráton do São Francisco: uma abordagem do ponto de vista da análise de bacias. M. Dominguez & A. Misi (ed.). *O Cráton do São Francisco*. Salvador, SBG/SGM/CNPq, p. 137-159

Dominguez J.M.L. & Rocha G.M.F. 1989. Seqüências deposicionais do Espinhaço Setentrional na região sudoeste do Estado da Bahia. Uma margem continental Proterozóica? In: Simpósio de Geologia de Minas Gerais. Belo Horizonte, *Anais*. Belo Horizonte, SBG. p. 190-194

Drumond J.B.V., von Sperling E., Raposo F.O. 1980. *Projeto Porteirinha-Monte Azul*. Belo Horizonte, DNPM-CPRM, 559p

Ernst R.E., Wingate M.T.D., Buchan K.L., Li Z.X. 2008. Global record of 1600–700 Ma Large Igneous Provinces (LIPs): implications for the reconstruction of the proposed Nuna (Columbia) and Rodinia supercontinents. *Precambrian Research*, **160**:159-178.

Fernandes P.E.C.A., Montes M.L., Braz E.R.C, Montes A.S.L, Silva L.L, Oliveira F.L.L, Ghignone J.I, Siga Jr O., Castro H.E.F. 1982. *Folha SD.23 Brasília, In*: Projeto Radam Brasil. Levantamento de Recursos Minerais (texto explicativo), **29**:25-204.

Gehrels G. 2011. Detrital zircon U–Pb geochronology: current methods and new opportunities. *In*: Busby, C., Azor, A. (Eds.), Tectonics of Sedimentary Basins. Blackwell Publishing Ltd., UK, p. 45–62

Gerdes A. & Zeh A., 2006. Combined U–Pb and Hf isotope LA-(MC-)ICP-MS analyses of detrital zircons: comparison with SHRIMP and new constraints for the provenance and age of an Armoricanmetasediment in central Germany. *Earth Planet Science Letter*, **249**:47-61.

Gower C.F. & Krogh T.E., 2002. A U–Pb geochronological review of the Proterozoic history of the eastern Grenville Province. *Canadien Journalof Earth Science*, **39**:795-829.

Gradim R.J., Alkmim F.F., Pedrosa-Soares A.C., Babinski M., Noce C.M. 2005. Xistos verdes do Alto Araçuaí, Minas Gerais: Vulcanismo básico do rifte Neoproterozoico Macaúbas. Revista Brasileira Geociências, **35**:59-69.

Guadagnin F., Chemale Jr. F., Magalhães A.J., Santana A., Dussin I., Takehara L. 2015. Age constraints on crystal-tuff from the Espinhaço Supergroup - Insight into the Paleoproterozoic to Mesoproterozoic intracratonic basin cycles of the São Francisco Craton. *Gondwana Research*, **27**:363-376.

Haughton P. 2001. Contained turbidites used to track sea bed deformation and basin migration, Sorbas basin, south-east Spain. *Basin Research*, **13**(2):117-139.

Haughton P.D.W., Barker S.P., McCaffrey W. 2003. 'Linked' debrites in sand-rich turbidite systems – origin and significance. *Sedimentology*, **50**:459-482.

Haughton P.D.W, Davis C., McCaffrey W., Barker S.P. 2009. Hybrid sediment gravity flow deposits – Classification, origin and significance. *Marine and Petroleum Geology*, **26**:1900-1918.

Hoffman P.F. 1991. Did the breakout of Laurentia turn Gondwanaland inside out? *Science*, **252**:1409-1412.

Hubbard S.M., Fildani A., Fomans B.W., Covault, J.A., and Mchargue T.R. 2010. High-relief slope clinoform development: insights from outcrop, Magallanes Basin, Chile: *Journal of Sedimentary Research*, **80**:357-375.

Inda H.A.V. & Barbosa J.F. 1978. Texto explicativo para o mapa geológico do Estado da Bahia, escala 1:1.000.000. Salvador, SME/CPM, 137 p.

Jackson S.E., Pearson N.J., Griffin W.L., Belousova E.A. 2004. The application of laser ablation-inductively coupled plasma-mass spectrometry to in situ U–Pb zircon geochronology. *Chemical Geology*, **211**:47-69

Johnson S.D., Flint S.S., Hinds D., Wickens H.V. 2001. Anatomy of basin floor to slope turbidite systems, Tanqua Karoo, South Africa: sedimentology, sequence stratigraphy and implications for subsurface prediction. *Sedimentology*, **48**:987-1023

Karfunkel J. & Hoppe A., 1988. Late Precambrian glaciation in central eastern Brazil: synthesis and model. *Palaeogeography, Palaeoclimatology, Palaeoecology*, **65**:1-21

Karfunkel J. & Karfunkel B. 1976. Estudos petro-faciológicos do Grupo Macaúbas na porção mediana da Serra do Espinhaço, Minas Gerais. In: Congresso Brasileiro de Geologia 29, Ouro Preto, *Anais,* 2. Sociedade Brasileira de Geologia, 179-188

Karfunkel J., Pedrosa-Soares A. C., Dossin I. A. 1985. O Grupo Macaúbas em Minas Gerais: revisão dos conhecimentos. Boletim do Núcleo Minas Gerais–Sociedade Brasileira de Geologia, **5**:45-59

Knauer L.G., Silva L.L, Souza F.B.B, Silva L.R. Carmo R.C. 2007. Folha Monte Azul, SD.23-Z-D-II, 1:100.000. *Programa Levantamentos Geológicos Básicos*. Texto explicativo e mapas. Belo Horizonte, UFMG/CPRM, 72p.

Kuchenbecker M., Pedrosa-Soares A.C., Babinski M., Fanning M. 2015. Detrital zircon age patterns and provenance assessment for pre-glacial to post-glacial successions of the Neoproterozoic Macaúbas Group, Araçuaiorogen, Brazil. *PrecambrianResearch*, **266**:12-26.

Lash G.G. & Blood D.R., 2014. Organic matter accumulation, redox, and diagenetic history of the Marcellus Formation, southwestern Pennsylvania, Appalachian basin. *Marine and Petroleum Geology*, **57**:244-263.

Leite M.M. 2013. *Sistema deposicionais e estudos de proveniência sedimentar do Supergrupo Espinhaço e do Grupo Macaúbas na porção ocidental do Anticlinal de Itacambira (MG)*. MS Dissertation. Instituto de Geociências, Universidade Federal de Minas Gerais, Belo Horizonte, 102p.

Li Z.X., Bogdanova S.V., Collins A.S., Davidson A., De Waele B., Ernst R.E., Fitzsimons I.C.W., Fuck R.A., Gladkochub D.P., Jacobs J., Karlstrom K.E., Lul S., Natapovm L.M., Pease V., Pisarevsky S.A., Thrane K., Vernikovsky V., 2008. Assembly, configuration, and break-up history of Rodinia: a synthesis. *Precambrian Research*, **160**:179-210.

Link M.H. 2003. Depositional systems and sedimentary facies of the Miocene-Pliocene Ridge Basin Group, Ridge Basin, southern California. In: Crowell, J.C.(ed.), Evolution of Ridge Basin, southern California: An interplay of sedimentation and tectonics: Boulder, Colorado. *Geological Society of America Special Paper*, **367**:17-87.

Lombello J.C., Pinheiro M.A.P., Queiroz S.F., Rojas J.N. Pinho J.M.M. 2014. *Folha SD.23-Z-D-V-4 Nova Aurora, escala 1:50.000*. Belo Horizonte, Serviço Geológico do Brasil, CPRM, Projeto Geologia do Brasil

Lowe D.R. 1982. Sediment gravity flows: II Depositional models with special reference to the deposits of high-density turbidity currents. *Journal of Sedimentary Research*, **52**:279-297.

Ludwig K.R. 2003. User's Manual for Isoplot/Ex, Version 3.0, A geochronological toolkit for Microsoft Excel. *Berkeley Geochronology Center Special Publication* 4, 73p.

Martins M., Karfunkel J., Noce C. M., Babinski M., Pedrosa-Soares A.C., Cial A.N., Liu D. 2008. A sequência pré-glacial do Grupo Macaúbas na área-tipo e o registro da abertura do rifte Araçuaí. *Revista Brasileira de Geociências*, **38**(4):761-772.

Martins-Neto M.A., Pedrosa-Soares A.C., Lima S.A.A. 2001. Tectono-sedimentary evolution of sedimentary basins from Late Paleoproterozoic to Late Neoproterozoic in the São Francisco Craton and Araçuaí fold belt, eastern Brazil. *Sedimentary Geology*, **141-142**:343-370.

Meert J.G. 2001.Growing Gondwana and rethinking Rodinia: a paleomagnetic perspective. *Gondwana Research*, **4**:279-288.

Menezes R.C.L., Conceicão H., Rosa M.L.S., Macambira M.J.B., Galarza M.A., Rios D.C. 2012. Geoquímica e geocronologia de granitos anorogenicos tonianos (c.914–899 Ma) da Faixa Araçuaí no Sul do Estado da Bahia. *Geonomos*, **20**:1-13

Miall A.D., 1996. The Geology of Fluvial Deposits: sedimentary facies, basin analisys and petroleum geology. Toronto. Springer Verlag, 582p.

Moraes L.J. 1929. Geologia da região diamantina de Minas Gerais. *In*: Relatório Anual do Diretor 1928, Rio de Janeiro. Serviço Geológico e Mineralógico, p. 29-34.

Moraes L.J. & Guimarães D. 1931. The diamond-bearing region of Northern Minas Gerais, Brazil. *Economic Geology:* **26**:502-530.

Moutinho da Costa L.A. (coord.) 1976. Projeto Leste do Tocantins/ Oeste do Rio São Francisco - LETOS. Relatório Final Integrado. Rio de Janeiro, PROSPEC S/A, convênio DNPM/CPRM, 557p.

Mulder T. & Alexander J. 2001. The physical character of subaqueous sedimentary density flows and their deposits. *Sedimentology*, **48**:269-299.

Mulder T, Syvitski J, Migeon S, Faugeres J. C, Savoye B. 2003. Marine hyperpycnal flows: Initiation, behavior and related deposits. A review. *Marine and Petroleum Geology*, **20**:861-82.

Mutti E. 1992. Turbiditesandstones. Agip, Instituto di geologia, Universitàdi Parma. p. 275.

Noce C.M., Pedrosa-Soares A.C., Grossi-Sad J.H., Baars F.J., Guimarães M.V., Mourão M.A.A., Oliveira M.J.R., Roque N.C. 1997. Nova Subdivisão Estratigráfica Regional do Grupo Macaúbas na Faixa Araçuaí: o registro de uma bacia neoproterozóica. In: SBG, Simpósio de Geologia de Minas Gerais, 9, Ouro Preto, *Anais*, **14**:29-31.

Noda A. & Toshimitsu S. 2009. Backward stacking of submarine channel–fan successions controlled by strike-slip faulting: The Izumi Group (Cretaceous), southwest Japan. *Lithosphere*, **1**(1):41-59

Pedrosa-Soares A.C., Alkmim F.F., Tack L., Noce C.M., Babinski M., Silva L.C., Martins-Neto M.A. 2008. Similarities and differences between the Brazilian and African counterparts of the Neoproterozoic Araçuaí-West Congo orogen. Geological Society, London, Special Publications, 294p..

Pedrosa-Soares A.C., Babinski M., Noce C., Martins M., Queiroga G., Vilela F. 2011. The Neoproterozoic Macaúbas Group (Araçuaí orogen, SE Brazil) with emphasis on the diamictite formations. *In*: Arnaud, E., Halverson, G. P. & Shields-Zhou, G. (eds). *The Geological Record of Neoproterozoic Glaciations*. Geological Society, London, Memoirs, **36**:523-534.

Pedrosa-Soares A.C., Noce C.M., Vidal P., Monteiro R.L.B.P., Leonardos O.H. 1992. Toward a new tectonic model for the Late ProterzoicAraçuaí (SE Brazil) - West Congolian (SW Africa) Belt. *Journal of South American Earth Sciences*, **6**:33-47.

Pedrosa-Soares A.C., Noce C.M., Wiedemann C.M., Pinto C.P. 2001. The Araçuaí-West Congo orogen in Brazil: An overview of a confined orogen formed during Gondwanland assembly. *PrecambrianResearch*, **110**:307-323.

Pedrosa-Soares A.C., Vidal P., Leonardos O.H., Brito-Neves B.B. 1998. Neoproterozoic oceanic remnants in eastern Brazil: Further evidence and refutation of an exclusively ensialic evolution for the Araçuaí-West Congo Orogen. *Geology*, **26**:519-522

Peixoto E.N., Pedrosa-Soares A.C., Alkmim F.F., Dussin I.A. 2015. A suture–related accretionary wedge formed in the Neoproterozoic Araçuaíorogen (SE Brazil) during Western Gondwanaland assembly. *Gondwana Research*, **27**: 878-896.

Petri S., Coimbra A.M., Amaral G., Ojeda H.O., Fúlfaro V.J., Ponçano W.P. 1986. Código Brasileiro de nomenclatura estratigráfica. *Revista Brasileira de Geociências*, **16**:372-376.

Pinheiro M.A.P., Lombello J.C., Queiroz S.F., Cuzzati T., Pinho J.M.M. 2014. *Folha SD.23-Z-D-II-4 Santo Antônio do Retiro,, escala 1:50.000*. Belo Horizonte, Serviço Geológico do Brasil, Projeto Geologia do Brasil.

Postma G., Nemec W., Kleinspehn K.L. 1988. Large floating clasts in turbidites: a mechanism for their emplacement. *Sedimentary Geology*, **58**:47-61.

Poyatos-Moré M., Jones G.D., Brunt R.L. Hodgson D.M., Wild R.J., Flint A.S. 2016. Mud-dominated basin-margin progradation: processes and implications. *Journal of Sedimentary Research*, **86**:863878

Prélat A., Hodgson D.M., Flint S.S. 2009. Evolution, architecture and hierarchy of distributary deep-water deposits: A high-resolution outcrop investigation from the Permian Karoo Basin, South Africa. *Sedimentology*, **56**:2132-2154.

Queiroga G.N. 2010. *Caracterização de restos de litosfera oceânica do Orógeno Araçuaí entre os paralelos 17° e 21°S*. PhD Thesis, Universidade Federal de Minas Gerais, Belo Horizonte.

Queiroga G. N., Dussin I.A., Martins M., Machado M.C., Kawashita K., Chemale F. 2012. Roteiro de Campo – Rochas Ígneas. In: Dussin I.A. &Chemale F. (ed). Geologia Estrutural e Estratigrafia do Sistema Espinhaço–Chapada Diamantina e sua Aplicação nas Bacias Mesocenozóicas da Margem Passiva Brasileira. Belo Horizonte, FUNDEP/PETROBRÁS, 170-195.

Queiroga G.N., Pedrosa-Soares A.C., Noce C.M., Alkmim F.F., Pimentel M.M., Dantas E., Martins M., Castañeda C., Suita M.T.F., Prichard H. 2007. Age of Ribeirão da Folha ophiolite, Araçuaí Orogen: the U-Pb zircon (LA-ICPMS) dating of a plagiogranite. *Geonomos*, **15**(1):61-65.

Queiroz S.F, Pinheiro M.A.P., Lombello J.C., Rojas J.N., Pinho J.M.M. 2014. *Folha SD.23-Z-D-V-2Rio Pardo de Minas, escala 1:50.000*. Belo Horizonte, Serviço Geológico do Brasil, Projeto Geologia do Brasil.

Ragan D.M. 2009. Structural Geology: An Introduction to Geometric Techniques (4a Ed.). Cambridge University Press, Cambridge, 602 p.

Reading H.G. & Richards M. 1994. Turbidite systems in deep-water basin margins classified by grain size and feeder system. *American Association of Petroleum Geologists Bulletin*, **78**(5):792-822.

Reis H.L.S., Alkmim F.F., Fonseca R.C.S., Nascimento T.C., Suss J.F., Prevatti L.D. 2017.The São Francisco Basin. *In*: Heilbron M., Cordani U.G., Alkmim F.F. (eds.). *São Francisco Craton, Eastern Brazil: Tectonic Genealogy of a Miniature Continent*, Brazil, Springs, p. 117-145

Salvador A. 1994. Lithostratigraphic units. In: Salvador A. (ed.) International Stratigraphic Guide. A guide to stratigraphic classification, terminology and procedure.Geological Society of America (International Subcomission on Stratigraphic Classification of International Union of Geological Sciences – IUGS; International Comission on Stratigraphy), 214p.

Sato T., Sawaki Y. Asanuma H., Fujisaki W., Okada Y., Maruyama S., Isozaki Y., Shozugawa K., Matsuo M., Windley B.F. 2015. Redox condition of the late Neoproterozoic pelagic deep ocean: 57 Fe Mössbauer analyses of pelagic mudstones in the Ediacaran accretionary complex, Wales, UK. *Tectonophysics*, **662**:472–480

Schobbenhaus C. 1972. Relatório geral sobre a geologia da região setentrional da Serra do Espinhaço - Bahia Central. Recife, SUDENE/DRN/DG, 91 p.

Schobbenhaus C. 1993. *O Proterozóico Médio do Brasil com ênfase à região Centro-Leste: uma revisão*. PhD tesis. Universidade de Freiburg, Freiburg. 166p.

Schobbenhaus C. 1996. As tafrogêneses superpostas Espinhaço e Santo Onofre, Estado da Bahia: revisão e novas propostas. *Revista Brasileira de Geociências,* **26**(4):265-276.

Shields G.A. 2016. Earth system transition during the Tonian–Cambrian interval of biological innovation: nutrients, climate, oxygen and the marine organic carbon capacitor. In:Brasier, A. T., McIlroy, D. &McLoughlin, N. (eds*). Earth System Evolution and Early Life: a Celebration of the Work of Martin Brasier.* Geological Society, London, Special Publications, 448p.

Silva H.T.F. 1993. *Flooding surfaces, depositional elements, and surfaces, depositional elements, and accumulation rates: Characteristics of the Lower Cretaceous tectonosequence in the Recôncavo Basin, northeast Brazil.* Austin. Ph.D. thesis, University of Texas, 313p.

Silva L.C., Pedrosa-Soares A.C., Teixeira L.R. 2008. Tonian rift-related, A-type continental plutonism in the Araçuaí orogen, Eastern Brazil: new evidences for the breakup stage of the São Francisco–Congo Paleocontinent. *Gondwana Research,* **13**: 527-537.

Sláma J., Kosler, J., Condon D.J., Crowley J.L.,Gerdes A., Hanchar J.M., Horstwood M.S.A., Morris G.A., Nasdala L., Norberg N., Schaltegger U., Schoene B., Tubrett M.N., Whitehouse M.J. 2008. Plesovice zircon – a new natural reference material for U–Pb and Hf isotopic microanalysis. *Chemical Geology,* **249**:1-35.

Sousa F. R., Santos E.L., Jesus M.T., Medeiros V.C. 2014. *Carta Geológica da Folha Mansidão, escala 1:1.000.000.* Teresina, Serviço Geológico do Brasil, Programa Geologia do Brasil.

Sousa M.E.S. 2016. *Caracterização Litoestrutural e Geocronológica dos Xistos Verdes e Metagabros do Grupo Macaúbas na Faixa Terra Branca - Planalto de Minas, Minas Gerais.* MS Dissertation, Departamento de Geologia/Escola de Minas, Universidade Federal de Ouro Preto, Ouro Preto, 215p.

Souza J.D., Kosin M., Heineck C.A., Lacerda Filho J.V., Teixeira L.R., Valente C.R., Bento R.V., Borges V.P., Santos R.A., Guimarães J.T., Leite C.A.S., Neves J.P., Carvalho L.M., Oliveira I.W.B., Pereira L.H.M. 2003. Folha SD. 23-Brasília. In: Schobbenhaus, C., Gonçalves, J.H., Santos, J.O.S., Abram, M.B., Leão Neto, R., Matos, G.M.M., Vidotti, R.M. (Eds.). Carta Geológica do Brasil ao Milionésimo, Programa de Levantamentos Geológicos Básicos do Brasil, CPRM, 2004, Brasília (Sistema de Informações Geográficas. Programa Geologia do Brasil). CD-ROM.

Spencer C.J., Kirland C.L., Taylor R.J.M. 2016. Strategies towards statiscally robust interpretations of in situ U-Pb zircon geochronology. *Geoscience Frontiers*: **7**:581-589

Surlyk F. 1984. Fan-delta to submarine fan conglomerates of the Volgian-Valanginian Wollaston Forland Group, East Greenland. In: Koster, E.H., and STEEL, R.J (eds.) Sedimentology of Gravel sand Conglomerates. *Memorial Canadian Society Petroleum Geology,* **10**:359-382.

Talling P.J., Masson D.G., Sumner E.J., Malgesini G. 2012. Subaqueous sediment density flows: Depositional processes and deposit types. *Sedimentology,* **59**:1937-2003

Tinterri R., Laporta M., Ogata K. 2017. Asymmetrical cross-currentturbidite facies tract in a structurally-confined mini-basin (Priabonian-Rupelian, Ranzano Sandstone, northern Apennines, Italy). *Sedimentary Geology,* **352**:63-87.

Trompette R. 1994. Geology of Western Gondwana (2000-500Ma). *Pan-African-Brasiliano aggregation of South America and Africa.* A.A. Balkema, Rotterdam, 350 p.

Uhlein A., Trompette R., Alvarenga C. 1999. Neoproterozoic glacial and gravitational sedimentation on a continental rifted margin: the Jequitaí-Macaúbas sequence (Minas Gerais, Brazil). *Journal of South American Earth Sciences,* **12**:435-451.

Uhlein A., Trompette R., Egydio-Silva M. 1998. Proterozoic rifting and closure, SE border of the São Francisco Craton, Brazil. *Journal of South American Earth Sciences,* **11**:191-203.

Uhlein A., Trompette R.R., Egydio-Silva M., Vauchez A. 2007. A Glaciação Sturtiana (~750 Ma), a estrutura do rifte Macaúbas-Santo Onofre e a Estratigrafia do Grupo Macaúbas, Faixa Araçuaí. *Geonomos,***15**(1):45-60.

van Achterbergh E., Ryan C.G., Jackson S.E., Griffin W. 2001. Appendix III. Data reduction software for LAICP-MS. *In*: Sylvester, P. (Ed.), Laser-ablation-ICP-MS in the Earth sciences, principles and applications. *Mineralogical Association of Canada.* Short Course Series, **29**:239–243

Vilela F.T., Pedrosa-Soares A.C., Carvalho M.T.N., Arimateia R., Santos E., Voll E. 2014. Metalogênese da Faixa Araçuaí: O Distrito Ferrífero Nova Aurora (Grupo Macaúbas, Norte de Minas Gerais) no contexto dos recursos minerais do Orógeno Araçuaí. In: Silva, M.G., Rocha-Neto, M.B., Jost, H., Kuyumjian, R.M. (Eds.), Metalogênese das Províncias Tectônicas Brasileiras, Rio de Janeiro, Brazil, p. 415-430

Viveiros J.F.M., Sá E.L., Vilela O.V., Santos O.M., Moreira J.M.P., Neto F.H., Vieira W.S. 1978. Geologia dos vales dos rios Peixe Bravo e alto Vacaria, norte de Minas Gerais. *In*: SBG, Congresso Brasileiro Geologia, Recife, 30, *Anais,* **1**:243-254.

Volkert R.A., Feigenson M.D., Mana S., Bolge L. 2015. Geochemical and Sr–Nd isotopic constraints on the mantle source of Neoproterozoic mafic dikes of the rifted eastern Laurentian margin, north-central Appalachians, USA. *Lithos,* **212-215**:202-213.

Zavala C. & Arcuri M. 2016. Intrabasinal and extrabasinalturbidites: Origin and distinctive characteristics. *Sedimentary Geology,* **337**:36-54.

Zavala C., Arcuri M., Gamero H., Contreras C., Di Meglio M. 2011. A genetic facies tract for the analysis of sustained hyperpycnal flow deposits. In: Slatt, R.M., Zavala, C. (Eds.), Sediment Transfer from Shelf to Deep Water — Revisiting the Delivery System. American Association of Petroleum Geologists, Studies in Geology, **61**:31-51.

Available at www.sbgeo.org.br